The relationship between cadmium and phosphate in the Atlantic Ocean unravelled

Rob Middag[a,b,c*], Steven M.A.C. van Heuven[1], Kenneth W. Bruland[2], Hein J.W. de Baar[1]

[a] Department of Ocean Systems (OCS), NIOZ Royal Netherlands Institute for Sea Research, and Utrecht University, P.O. Box 59, 1790 AB Den Burg, Texel, The Netherlands

[b] Department of Ocean Sciences & Institute of Marine Sciences, University of California Santa Cruz, CA 95064, USA

[c] Department of Chemistry, NIWA/University of Otago Research Centre for Oceanography, Dunedin 9054, New Zealand

[*] corresponding author rob.middag@nioz.nl

Abstract

Cadmium (Cd) is not generally considered a nutrient element, but behaves like a nutrient in the oceans and might play an important role in ocean biology after all. The relationship between Cd and the nutrient phosphate (PO_4) has been studied for over 40 years, but the debate on the driving mechanism and reason behind the 'kink', a change in the steepness of the slope is ongoing. Using new data of high accuracy and spatial resolution covering the West-Atlantic Ocean from north to south, in combination with a robust extended optimum multiparameter (eOMP) water mass model, we show that mixing between different water masses is the dominant factor explaining the observed correlation and its kink. Regeneration of Cd via remineralisation explains the smaller scale variability, notably in the surface ocean. Observations imply the availability of Cd in surface waters determines the Cd-uptake and thus the Cd:PO_4 remineralisation ratio. This ratio is variable between different ocean regions, notably between the northern and southern high latitude oceans. Due to their role in deep water formation, both the northern and southern high latitude oceans are a driving factor in the Atlantic and global Cd and PO_4 relation. Outside the Atlantic Ocean, the classical kink is not expected, but the relationship is by no means linear. Most likely, this is due to the interaction between low latitude surface waters and subsurface waters from high latitude origin, but more data are required to assess this in detail.

Keywords: GEOTRACES; Cadmium; Phosphate; Atlantic; extended optimum multiparameter analysis

1. Introduction

Dissolved trace metals in the oceans occur at low concentrations, yet many are essential for life as trace nutrients while others are valuable tracers of ocean processes (Bruland et al., 2014). The concentration of Cd in the ocean varies between < 1 pmol kg^{-1} in surface waters, up to ~1 nmol kg^{-1} in old deep waters (Fig. 1). Since the first accurate oceanic measurements

of dissolved Cd (Boyle et al., 1976; Bruland et al., 1978; Martin et al., 1976), marine scientists have been intrigued by the nutrient-type distribution of Cd as Cd was deemed to be a non-essential trace metal element for biota.

The mechanism of Cd-removal from surface waters is subject of debate but is clearly coupled to biological processes e.g. (Horner et al., 2013; Morel, 2013). A biological role for Cd as a co-factor in a Cd-specific carbonic anhydrase enzyme has been identified in some phytoplankton species, notably diatoms (Lane and Morel, 2000). Other species that do not possess this Cd-enzyme have been shown to be able to substitute Zn or Co with Cd in the carbonic anhydrase enzyme (Morel, 2013; Xu et al., 2007). This plasticity via metal substitution has likely evolved in the open ocean due to the sparing availability of bio-essential trace metal elements, and Cd addition can stimulate plankton growth e.g. (Price and Morel, 1990; Sunda and Huntsman, 2000). In contrast, Horner et al. (2013) argued that Cd uptake is non-specific, i.e. 'mistaken identity' were phytoplankton are unable to differentiate between Cd and bio-essential divalent metals. The Cd is subsequently bound and stored inside the cell to avoid toxicity, coupling the cycling of Cd to the biological cycle of nutrients. Regardless of the actual underlying mechanism, it is clear that in the surface ocean there is net removal of Cd by phytoplankton that is returned into solution in the subsurface waters via remineralisation, leading to the coupling of the distributions of Cd and PO_4.

The relationship between Cd and PO_4 is distinctly bi-linear (Fig. 1) and has often been described as having a 'kink', a change in the steepness of the slope, at a PO_4 concentration of ~1.3 μmol kg^{-1} (Cullen, 2006; De Baar et al., 1994). The origin of this kink in the Cd-PO_4 relations is, akin to the uptake of Cd, subject to scientific debate. The data to the left of the kink (i.e. PO_4<1.3 μmol kg^{-1}) is generally from surface waters and relatively young deep North Atlantic waters and the Cd-PO_4 linear regression tends to go through the origin of the graph (Fig. 1). Data to the right of the kink (i.e. PO_4>1.3 μmol kg^{-1}) is from the deep (deeper

than 1000 m) waters from the Indian, Pacific and Southern oceans (De Baar et al., 1994), but the current GEOTRACES data shows this division is an oversimplification (Fig. 1). The regression to the right of the kink has a non-zero intercept i.e. there is 'left-over' PO_4 at zero Cd. This non-zero intercept leads to an increasing dissolved Cd/PO_4 ratio with increasing concentrations of these elements. Since the concentrations of these nutrient elements increase with water mass age, older water masses will have a higher Cd/PO_4 ratio. The latter ratio is referred to as the dissolved ratio or "spot ratio" and should not be mistaken with the apparent uptake or remineralisation ratio that can be deduced from the slope of the regression $\Delta Cd/\Delta PO_4$ in the surface and deep ocean, respectively e.g. (Abe et al., 2006; Baars et al., 2014). In this paper Cd/PO_4 will be used to indicate a spot ratio, $Cd{:}PO_4$ to denote either a ratio of particles, and/or an uptake or remineralisation ratio. The slope of the regression should fit data over the entire water column and ideally be equivalent to the ratio in the particles. This only holds if both elements are taken up and remineralised in perfect harmony without influence of other processes, such as mixing of water masses with a different spot ratio and/or different remineralisation ratio. For Cd, this idealised concept is clearly not the case given the kinked relationship. Preferential remineralisation of PO_4 over Cd has been suggested as the cause of the kink in the $Cd\text{-}PO_4$ relationship (Boyle, 1988), as has the influence of Sub-Antarctic waters depleted in Cd (Frew and Hunter, 1992; Xie et al., 2015) and relatively Cd-rich Antarctic Bottom Water (AABW) (Frew, 1995). Additionally, increased Cd uptake under limitation of bio-essential trace metal elements (notably Fe, Zn, Mn) (Cullen, 2006; Quay et al., 2015; Sunda and Huntsman, 2000 and references therein), as well as the influence of CO_2 concentrations (Cullen et al., 1999) have been suggested to explain the higher Cd/PO_4 ratios in Antarctic origin water. The driving role of the Southern Ocean for the macronutrient distribution of the Atlantic Ocean is well established (Sarmiento et al., 2004) and recent studies show the importance of Antarctic origin water and water mass

mixing for trace elements and isotopes as well (e.g Vance et al., 2017; Wyatt et al., 2014; Xie et al., 2015).

Thus far most work on the Cd-PO_4 relationship has relied on regional studies or data compilations. The campaign of four consecutive GEOTRACES cruises (2010-2012) in the West Atlantic Ocean offered the opportunity to unravel and elucidate the remarkable coupling of Cd and PO_4 along the conduit of the southward travelling deep North Atlantic water and the northward travelling waters of Antarctic origin. The Cd measurements were all performed by the same analyst and the shipboard PO_4 measurements were done by members from the NIOZ nutrient laboratory that specialises in high accuracy nutrient measurements. This generated a large, internally consistent, dataset such that the interpretations can more optimally be attributed to oceanic processes rather than being hampered by analytical variability. Additionally, an extended Optimum Multiparameter (eOMP) analysis was done to separate the contributions of the main water masses in the West Atlantic Ocean, allowing us to unravel the effects that the distributions and mixing of the different water masses have on the distributions of dissolved Cd and PO_4 and the Cd-PO_4 relationships. The high sampling resolution of 24 depths per station and the data from overall 60 station positions (Fig. 2) provides the opportunity to assess the cycling of Cd and its relationship with PO_4 for the entire West Atlantic basin. Here the West Atlantic basin was chosen for the unique overall 17,500 km long full depth section, as the West Atlantic is the main pathway of the deep ocean conveyor belt driving deep ocean circulation.

2. Material and methods

2.1 Water sample measurements

Samples were collected along the Netherlands GEOTRACES GA02 transect during four consecutive expeditions (2010–2012). Sampling was done with an all-titanium ultraclean CTD sampling system for trace metals with novel PVDF samplers (Rijkenberg et al., 2015).

All Cd data in this paper is dissolved Cd. The accuracy of the Cd determination was verified by using reference seawater and cross-over stations, demonstrating the Cd data is consistent with the data from the US GEOTRACES zonal Atlantic section (Middag et al., 2015) and the data and metadata are available in the GEOTRACES Intermediate Data Product (Mawji et al., 2015). Additional details on sampling and analysis for Cd, nutrients and hydrographical parameters can be found in the supplementary material.

2.2 The extended optimum multiparameter (eOMP) analysis

The contributions of 7 pre-defined *end-member* water masses (composed of 11 water types (Tomczak, 1981)) to each measured water sample were quantified using optimum multiparameter (OMP) analysis (Mackas et al., 1987; Tomczak, 1981). Consideration of the effects of remineralisation, expressed as the deficit of oxygen *D*, allows our analysis to be applied over large spatial scales (Karstensen and Tomczak, 1998). Remineralisation mainly occurs in the depth zone extending from just below the upper mixed layer to shallower than 1000m (Fig. S2). The amount of remineralisation that has occurred relative to the end-member mixture, is inferred as part of the eOMP procedure, and is expressed as an oxygen deficit. This deficit of oxygen is relative to the inferred source water type mixture, as opposed to AOU which represents consumption relative to atmospheric equilibrium, i.e. $D = O_{2\ mixing} - O_{2\ observed}$ (where $O_{2\ mixing}$ is the O_2 concentration one would expect based on conservative mixing of endmembers). Endmember characteristics for S, T, O_2, Si and NO_3 (Table S1) are defined through analysis of section plots and property-property plots and generally correspond to water mass characteristics observed at the extremities of our ocean section. For some water masses this does not correspond to their physical formation regions, but this has the advantage that we do not have to rely on measurements from other datasets (if available at all) or account for processes that occur outside our sampling region and cannot be assessed with accompanying data. Thus to distinguish mixing processes from biogeochemical processes in

126 our study region, water mass definitions ‘at the position of entry into our study region’ are
127 preferred.

128 Restrictions were imposed on the presumed spatial extent of water types in order to limit the
129 number of types to be considered to contribute to a sample, so as not to underconstrain the
130 eOMP solution (Table S2). Remineralisation ratios $\Delta P:\Delta N:\Delta O_2$ were set at 1:16:-170
131 (Anderson and Sarmiento, 1994), while $\Delta Si:\Delta O_2$ (which is known to vary vertically (Hupe
132 and Karstensen, 2000)), was assumed to be a fixed 1:-34, (i.e., $\Delta P:\Delta Si = 1:5$). Phosphate was
133 excluded as an independent variable from the eOMP. Figures illustrating eOMP results and
134 robustness of the results may be found in the supplementary material.

135 To demonstrate the veracity of the eOMP method, values of PO_4 were predicted from inferred
136 water type contributions, inferred oxygen deficit *D*, a $\Delta P:\Delta O_2$ of 1:-170 and assigned PO_4
137 end-member values. The predicted PO_4 values closely correspond to measurements (R^2 =
138 0.97, root mean square error (rmse) = 0.11 µmol kg^{-1}). Values of Cd were at first predicted
139 only from water mass contributions and the assigned Cd endmember values, without
140 accounting for input by remineralisation. This already resembles measured Cd, quite well
141 including the kink at PO_4 = 1.3 µmol kg^{-1} (see section 3.3).

142 Subsequently, remineralisation was accounted for (using literature $\Delta Cd:\Delta O_2$) followed by
143 deriving an optimised set of Cd endmember definitions and an optimised $\Delta Cd:\Delta O_2$
144 remineralisation ratio via inversion of the system (see section 3.3 and supplementary
145 material). The eOMP results were calculated with a non-negativity constraint for the
146 optimised Cd endmembers. We employed the same optimisation procedure for PO_4
147 endmembers and the $\Delta PO_4:\Delta O_2$ remineralisation ratio. This yields a ratio of 1:-173 and
148 endmembers close to those estimated based on the observations (Table S5), indicating this
149 method functions appropriately. Water samples are considered to be of northern origin if the
150 sum of fractional contributions of North Atlantic Deep Water (NADW) and North Atlantic

Central Water (NACW) is larger than 0.5. All other samples are considered to be of southern origin.

3. Results and Discussion

3.1 Hydrography

The hydrography along the section has been described by Middag et al. (2015) and is expanded here with additional detail on intermediate and mode waters as well as the basin wide circulation (Fig. 2). The North Atlantic Sub-Polar Mode Water (NASPMW) is observed as surface water in the northernmost part of the transect in the wind driven North Atlantic Sub-Polar Gyre and as subsurface water southwards. The deepest water mass here is the southward flowing NADW. Around the Grand Banks (~45 °N), there is the transition to the warmer surface NASTMW in the North Atlantic Sub-Tropical Gyre (NASTG). Both NASPMW and NASTMW are considered components of the NACW. Fresher Equatorial Surface Water (ESW) was observed between ~30°S and 30°N along the current transect. Around the equator between ~20°N and ~15°S at depths between ~ 100 and 1000 m an Oxygen Minimum Zone (OMZ) is observed. This OMZ is the result of local primary production and subsequent decay at the OMZ depth, as well as advection of low-oxygen water from the east, notably the strong OMZ near the Cape Verde Islands and the OMZ in the Angola Gyre (Rijkenberg et al., 2014).

The deepest, near bottom water mass in the Northern Hemisphere (NH) is a remnant of AABW that was formed by deep water formation around Antarctica and flows northward a as a cold, dense, nutrient rich water layer. The AABW is also referred to as Lower Deep Water in the North Atlantic, but here will be referred to as AABW to underline its Antarctic origin.

In the Southern Hemisphere (SH) two additional nutrient rich Antarctic water masses, Antarctic Intermediate Water (AAIW) and upper Circumpolar Deep Water (uCDW) advect northward at intermediate depth in between the overlying South Atlantic Central Water

(SACW) and ESW and the underlying southward flowing NADW. South Atlantic Sub-Polar Mode Water (SASPMW) is present as surface water south of the South Atlantic Sub-Tropical Gyre (SASTG) and as subsurface water north thereof. SASTMW and SASPMW are precursors or source waters of SACW (Stramma and England, 1999) but for simplicity here considered components of SACW (akin to NASPMW and NASTMW for NACW).

Two water masses that have been suggested to be of special importance for the distribution of Cd are AAIW and SASPMW (Xie et al., 2015). The latter is also referred to more generally as Sub Antarctic Mode Water (SAMW) and this water mass is also present in the Pacific and Indian oceans. Around Antarctica, CDW upwells and subsequently advects northwards. North of the Polar Front this surface water subducts as AAIW at the Sub-Antarctic Front (SAF) and continues to advect equatorward. North of the SAF, winter time mixing of surface water with the underlying water, creates the SAMW that is dense enough to subduct, but less dense than the underlying AAIW. It should be realised that for both SAMW (SASPMW in the Atlantic) and AAIW, different types are recognised, depending on their formation region and processing. For example, AAIW formed in the Indian Ocean also influences the Atlantic Ocean, it enters around South Africa and reaches the West-Atlantic with the Benguela Current as well as via the equatorial currents. During northward advection, the SASPMW and AAIW mix through diapycnal mixing with one another as well as with the overlying thermocline waters and with the underlying nutrient rich uCDW with relatively low oxygen and salinity (Van Aken, 2007).

3.2 Observational results

The concentrations of dissolved Cd were depleted to < 10 pmol kg^{-1} in the surface ocean along the transect, with the exception of the northern and southern end (Fig. 2). South of 45°S, surface concentrations increase to ~60 pmol kg^{-1} and from around 44°N northwards, concentrations increased from < 10 pmol kg^{-1} to >200 pmol kg^{-1} around 64°N. This northward

and southward increase in Cd continues beyond the current transect, to surface concentrations up to ~600 pmol kg^{-1} in the Atlantic section of the Southern Ocean (Baars et al., 2014) and around ~300 pmol kg^{-1} in the Canadian basin of the Arctic Ocean (Cid et al., 2012). Depleted surface Cd concentrations extend to greater depths around 30°N and 30°S in the subtropical gyres than at higher and lower latitudes. The shoaling of the Cd isolines towards the equator is probably the result of upwelling of deep water near the equator as well as the presence of STMW in the subtropical gyres that was formed from low [Cd] surface waters. Towards the higher latitudes, the inflow of high latitude water with relatively elevated [Cd] causes the observed shoaling of the isolines.

The data provides the opportunity to unravel the remarkable coupling of Cd and PO_4 along the path of the NADW flowing southward, and AABW and AAIW of Antarctic origin, flowing northward (Fig. 2b). At depth, the water masses of Nordic and Antarctic origin can be clearly distinguished based on their contrasting Cd and PO_4 (Fig. 2b,c). These new data clearly feature the kink at a PO_4 concentration of ~1.3 µmol kg^{-1} (Fig. 3a), as well as many samples deviating from the general relationship (mostly towards high PO_4 or low Cd). Upon closer inspection, several distinct apparent mixing lines can be distinguished in the dataset (Fig. 3b). In the low concentration range, distinct lines may be discerned for (line 1) the NASTMW, (line 2) the NASPMW, (line 3) the bulk NADW, and a nonlinear (3-watermass) mixing curve in the South Atlantic (curve 8). Mixing between the intermediate depth NADW with either the underlying AABW or the overlying AAIW occurs along two distinct mixing lines (lines 4 and 5, respectively). It is the differing slopes between regression lines 3 and 4 that constitutes the classical kink at a PO_4 of ~1.3 µmol kg^{-1}. To a lesser degree, there also exists a kink between regression lines 3 and 5. In the South Atlantic (SA), there are some striking differences compared to the North Atlantic (NA). Data from the SASTG surface exhibits a convex relationship between Cd and PO_4. South of the SASTG, two comparatively steep regressions

with distinctly non-zero intercepts can be fitted, one for the surface ocean (line 6) and one for the remainder of the water column (line 7). Strikingly, data from both deep and intermediate depth water masses of Antarctic origin fall along a single regression line (line 7). The convex relation (curve 8) observed in the shallow (0-500m) SA implies mixing between 3 endmembers: SASTMW surface water depleted in both Cd and PO_4, AAIW elevated in both Cd and PO_4 and SASPMW that has low Cd but intermediate PO_4 (Fig. 3b). Going from south to north, due to the dilution of the SASPMW endmember the curve becomes progressively less convex (i.e. more linear) until the influence of the OMZ is observed.

Summarising, all water masses of Antarctic origin traveling northwards largely plot along one steep regression (7) with a non-zero intercept until the equatorial region is reached and a second regression begins to appear (5), at comparatively lower Cd. Surface waters from the SA plot along one steep regression in the far south, but mixing between subtropical gyre surface water with the underlying SASPMW and AAIW gives rise to a convex relationship. In the NA, in the absence of an influence of Antarctic origin, some variation is observed, but the Cd-PO_4 relationship is largely linear with a near-zero intercept as also observed by Roshan and Wu (2015). The classical kink appears when NADW of northern origin begins to mix with water of Antarctic origin, this implying that the mixing of different water masses governs the deep Cd-PO_4 relation. The variation in the overall dataset is partly based on water mass mixing and partly based on the preceding, pre-mixing, life history of the water masses. This has been suggested previously (e.g. (Abouchami et al., 2011; Conway and John, 2015; Xie et al., 2015), but is now evident from this long meridional transect where the influence of mixing and remineralisation can be better distinguished as will be done in the next section.

3.3 Modelling and remineralisation

Using the extended optimum multiparameter (eOMP) model, we infer fractional contributions of various source water types to samples. Values of Cd are predicted by straightforward

multiplication of these fractions with assigned endmember Cd values (estimated from the observations). The predicted Cd resembles the measured Cd reasonably well (Fig. 4a) for samples with low amounts of remineralisation (oxygen deficit <~60µmol kg^{-1}). About 86% of the variation in the observed Cd is explained by the mixing-only model (rmse Cd: ±80 pmol kg^{-1}). Moreover, using the mixing-only model, the classical kink at a PO_4 of ~1.3 µmol kg^{-1} is reproduced (Fig. 3c), conclusively demonstrating the kink is solely the result of mixing between water masses of various origins.

Remineralisation of particles returns Cd to the water column, explaining why the mixing-only model underestimates Cd for samples with a higher oxygen deficit. The model fit is markedly improved by accounting for the remineralisation process. Assuming an invariable Cd:-O_2 ratio of 2 pmol/µmol (based on previous estimates for the Atlantic Ocean (Roshan and Wu, 2015; Twining and Baines, 2013)), the explanatory power of the models is increased to ~95% (rmse Cd: ±48 pmol kg^{-1}; Fig. 4b). Allowing the model to infer both optimal Cd endmembers and the optimal Cd:O2 remineralisation ratio further improves the fit to ~98% (rmse Cd: ±32 pmol kg^{-1}), yielding Cd:-O_2=1.25±0.03 pmol/µmol (see supplementary material for uncertainty calculation). Lastly, we expand the model optimisation using individual remineralisation ratios for northern and southern origin waters. This results in different remineralisation ratios for northern and southern origin waters (1.14±0.03 pmol/µmol and 1.40±0.05 pmol/µmol respectively), but this did not meaningfully improve the fit, so no conclusions can be drawn from this observation. The optimised model reproduces the observations well with low residuals (generally to within 20 pmol kg^{-1}; Fig. 4c) for the majority of the transect but there are some larger deviations, mainly in the sub-surface waters of the SA (Fig. 5b). Due to the local mixing of high and low Cd-endmembers in this region, small errors in the eOMP solution here, lead to relatively large errors of the predicted Cd concentration. The inferred Cd:-O_2 remineralisation ratios can be converted to a Cd:PO_4

remineralisation ratio using a standard -O_2:PO_4 ratio (Anderson and Sarmiento, 1994) of -170:1. The resulting Cd:PO_4 remineralisation ratio of 0.21±0.01 nmol/µmol (0.21±0.02 nmol/µmol when accounting for the uncertainty in the -O_2:PO_4 ratio (170±10:1) in the conversion) that is inferred from the Cd-O_2 consumption relationship, is similar to the dissolved Cd/PO_4 ratio observed at the lower end of the thermocline (Fig. 5a).

The Cd/PO_4 ratio just below the thermocline was largely set during water mass formation and remineralisation of biogenic material in the northern and southern high latitudes. The driving role of the Southern Ocean is not surprising as this has been established for trace elements as well as isotopes (e.g. de Souza et al., 2014; Xie et al., 2017), but the role of the northern high latitude oceans as driver of trace element distributions has received less attention. For the deep Cd-PO_4 relationship, it is the difference between the Cd-PO_4 ratios in the northern and southern deep water endmembers that drives the relationship between the two elements (see section 3.2 and 3.3). This leads to the question what drives the differences between the endmembers (section 3.4), but first we will assess the cycling of Cd and PO_4 in the Atlantic Ocean and the resemblance between the dissolved Cd/PO_4 ratio in the subsurface water and the inferred Cd:PO_4 remineralisation ratio.

3.4 Supply from below and availability in the surface ocean

Realising that both Cd and PO_4 are largely supplied to the surface ocean from the underlying waters, it becomes apparent that the Cd:PO_4 remineralisation ratio, as inferred from the model, resembles the dissolved Cd/PO_4 ratio from the underlying waters. Here it should be noted the resemblance between the dissolved Cd/PO_4 ratio in underlying water and the inferred Cd:PO_4 remineralisation ratio might be coincidental and obviously depends on the arbitrary distinction between surface and underlying waters (Fig. 5a), but warrants further discussion nonetheless.

As both Cd and PO_4 are depleted in the surface ocean, virtually all Cd and PO_4 that is supplied, is also taken up and thus the average uptake ratio has to match the average supply ratio. Assuming all uptake is eventually remineralised as well, the average remineralisation ratio also has to match the supply ratio. This implies that if one assumes that supply from the subsurface is the dominant supply of Cd and PO_4 and that these elements remineralise in unison, a self-perpetuating cycle exists. The Cd and PO_4 availability in the surface ocean is set by the supply ratio from below and if both elements are (nearly) quantitatively depleted, the returning exported and remineralising particles have a Cd:PO_4 ratio similar to the supply ratio. This keeps the dissolved ratio in the subsurface ocean reasonably constant unless there is significant influence of a water mass with a different ratio or an external input. This can indeed be observed along the current transect from south to north where the Cd/PO_4 ratio below the thermocline is constant until ~15°N (Fig. 5a), coinciding with the transition between northern and southern origin water at intermediate depth (200-1000m, see Fig. S 2 and S3). Looking beyond the current transect, Baars et al. (2014) observed Cd/PO_4 ratios between 0.21 and 0.32 nmol/µmol in young SAMW and AAIW, which gives an average of 0.26 nmol/µmol. This is similar to the average and range observed for these water masses in the SA (Fig. 5a) and close to the model inferred remineralisation ratio. This does not conclusively prove the self-perpetuating cycle, but the idea that supply from below, availability and uptake in the surface layer and remineralisation in the subsurface can remain balanced during advection of water masses is a plausible concept. This implies a controlling role for the northern and southern high latitude oceans. Not only for the Cd-PO_4 relationship in the deep Atlantic, but also for the surface Atlantic as the high latitude oceans are the source regions of the subsurface water masses that supply nutrients to the low latitude Atlantic Ocean (Sarmiento et al., 2004).

Roshan and Wu (2015) applied an OMP model (where PO_4 was included as a variable) in combination with Cd data deeper than 300 m on a zonal transect in the NA. Compatible with this work, our results indicate an important role for remineralisation in delivering Cd to the surface ocean (~40% of total Cd), whereas deep ocean concentrations are nearly exclusively (~95%) determined by mixing of end members (Fig. 6). The Cd:PO_4 remineralisation ratio by Roshan and Wu (2015) was estimated based on the difference between (i) the observations and (ii) the Cd and PO_4 concentrations calculated using a mixing only model. For the current study, the ratio was estimated independently from PO_4, using the relationship between remineralised Cd and the oxygen consumption over the entire water column. Following these different approaches, reasonably similar Cd:PO_4 remineralisation ratios are calculated, 0.26 nmol/μmol by Roshan and Wu (2015) for the NA versus 0.21 nmol/μmol in the current study for the entire Atlantic. Compared to the zonal dataset, the current meridional data provides additional insight into the processes occurring during transport of water masses through the Atlantic and we explore the possibility of different remineralisation ratios in different regions. The latter could not be conclusively demonstrated with the current data set and eOMP (see section 3.3) for the different regions in the surface and subsurface Atlantic Ocean (NA and SA). However, the difference in the subsurface dissolved Cd/PO_4 ratios in waters from northern and southern origin (Fig 5a), which we suggest drive the uptake and remineralisation ratios, imply such a difference is plausible. Additionally, different remineralisation ratios in different regions probably also underpin the difference between the northern and Antarctic origin waters (deep water masses) as discussed in the following section.

3.5 Importance of high latitude oceans

The kink in the Cd-PO_4 relationship can be explained by mixing of Antarctic origin and NADW as suggested before (Frew, 1995; Frew and Hunter, 1992). However the underlying processes that lead to the different Cd:PO_4 ratios in the endmember water masses are still

uncertain. In culture studies, it has been observed for thee marine diatom species and a coccolithophore that an increasing free Cd concentration in the medium led to increased Cd contents of the phytoplankton cells (Sunda and Huntsman, 2000). For the sake of argument, we assume the uptake of Cd relative to PO_4 increases with increasing availability of Cd in the ocean as well, where we assume dissolved Cd is bioavailable. The NADW is formed in the northern high latitude regions, which is largely supplied by nutrient poor surface water transported north with the Gulf stream. This results in comparatively low Cd (~100-300 pmol kg^{-1}) in the surface and subsurface waters where NADW is formed. Notably in the Arctic Ocean, an important source region for of NADW (Rudels et al., 2000), Cd:PO_4 remineralisation ratios on the order of 0.2-0.3 nmol/μmol have been inferred (Cid et al., 2012; Danielsson and Westerlund, 1983). Contrarily, the Antarctic origin water masses are supplied by upwelling nutrient rich waters. Consequently, Cd is much higher in these waters (~150-650 pmol kg^{-1}), as is the Cd:PO_4 remineralisation ratio that is in the range of 0.48-0.65 nmol/μmol (Baars et al., 2014; calculated from their Cd* values, the mean remineralisation ratio reported was 0.54 nmol/μmol). These respective remineralisation ratios are in line with the remineralisation ratios inferred from the slopes of regression for the Cd-PO_4 relationships in NADW in the NA (slope ~0.29 nmol/μmol) and Antarctic origin water masses in the SA (slope ~0.46-0.67 nmol/μmol; Table S6), confirming the remineralisation signature imprinted in the formation regions gets transported to the Atlantic. The differing Cd availability in the northern and southern deep water formation regions could thus lead to different Cd:PO_4 ratios in remineralising organic matter and subsequently to different dissolved Cd/PO_4 ratios in the northern origin compared to southern origin waters, giving rise to the classical kink in the Cd-PO_4 relationship.

It has been suggested previously that in High Nutrient Low Chlorophyll (HNLC) regions such as the Southern Ocean, limitation of trace metal elements Fe (e.g. De Baar et al., 1995;

374 Klunder et al., 2011) or Mn (Browning et al., 2014; Middag et al., 2013) could lead to
375 increased Cd uptake due to increased use of Cd in biochemical processes and/or inadvertent
376 uptake due to up-regulation of metal transporters (Cullen, 2006; Sunda and Huntsman, 2000).
377 Additionally, both the availability of Zn and CO_2 have an effect as well (Cullen et al., 1999).
378 Specifically for the Southern Ocean, Baars et al. (2014) suggested that low levels of free Zn
379 relative to levels of free Cd in the formation region of AAIW and SAMW and low levels of
380 Mn and Fe further south could cause a high Cd uptake. The latter observations and concepts
381 provide a physiological explanation for the here suggested increased uptake of Cd under high
382 Cd concentrations. However, based on the current Atlantic dataset it is not possible to
383 conclude whether this drives the increased Cd uptake. Nevertheless, an increased Cd uptake is
384 only feasible if there is sufficient Cd available for uptake, regardless of the underlying driving
385 uptake mechanism. Therefore we postulate the elevated Cd availability is the dominant factor
386 in explaining the high Cd uptake in the Southern Ocean relative to the Nordic seas and Arctic
387 Ocean, thus explaining the difference Cd:PO_4 ratios between these endmembers. Given the
388 differences between the Cd-PO_4 relationship in NADW and the Antarctic origin waters, a
389 constant Cd:PO_4 ratio to calculate excess or missing Cd (often denoted as Cd*) does not seem
390 suitable as discussed in the next section.

391 3.6 Calculating Cd based on PO_4

392 At first glance, it would appear there is a PO_4 deficit in waters with a high oxygen deficit (Fig
393 3a). However, the observations in these oxygen-deficient waters (roughly between 150 and
394 500 m depth in the equatorial region) can be reproduced when accounting for remineralisation
395 (Fig. 4c and 5b). The AAIW and SASPMW endmembers have a relatively high dissolved
396 Cd/PO_4 ratio (Fig 5a and S4). Assuming remineralisation adds Cd and PO_4 in the inferred
397 remineralisation ratio (0.21 nmol/μmol), this results in a lower dissolved Cd/PO_4 ratio than
398 when taking the slope of the SA deep Cd-PO_4 regression (slope ~0.46-0.67 nmol/μmol; Table

S6) as the remineralisation ratio. Remineralisation in the high productivity equatorial SA with the inferred remineralisation ratio (0.21 nmol/μmol) would result in the separate regression for Antarctic bottom (line 4 in Fig 3b) and Antarctic intermediate waters (line 5 in Fig 3b) as observed in this dataset. Only the intermediate depth Antarctic origin waters are affected, as the majority of the remineralisation happens in the depth range occupied by those water masses, whereas only negligible remineralisation occurs in the bottom waters (Fig. 6). This explains why all Antarctic origin water plot along a single steep Cd-PO_4 regression when only considering the region south of the productive equatorial region, whereas intermediate depth (AAIW and UCDW) and deep (AABW) waters plot along different regressions for the equatorial region and northwards thereof.

Thus the apparent Cd-depletion with respect to PO_4 in the relatively high oxygen-deficit equatorial region in the West-Atlantic can in fact be explained as long as the Cd:PO_4 remineralisation ratio is not based on the slope of the deep Cd-PO_4 regression. This deep water regression reflects remineralisation in the source region, and not necessarily remineralisation in other regions like the Atlantic. The point here is that the choice of Cd:PO_4 remineralisation ratio strongly affects the identification of a Cd deficiency with respect to PO_4 and that, if possible, a local remineralisation ratio should be quantified and used. This is not inconsistent with previous studies that found loss of Cd due to scavenging in severely oxygen deficient waters (Conway and John, 2015; Janssen et al., 2014) as all oxygen concentrations along the current transect were > 75μmol kg^{-1}. In fact, Conway and John (2015) related the small Cd deficiency they observed in the northwestern Atlantic to the presence of AAIW. This is in agreement with our interpretation, but it is now apparent that the Cd/PO_4 ratio in AAIW changes during advection northward (Fig. 3b and 5a) due to mixing and possibly local (Atlantic) remineralisation with a Cd/PO_4 ratio that is different from the AAIW source region.

3.7 Relationship outside the Atlantic Ocean

As can be seen from the current data (Fig. 3b), the Cd-PO_4 relationship in the Atlantic Ocean in fact is comprised of multiple linear relationships as well as a convex relation (curve 8), rather than a bi-linear relationship. This implies multiple mixing lines, a variable Cd:PO_4 remineralisation ratio and remineralisation in waters with differing initial (i.e. before local remineralisation) dissolved Cd/PO_4 ratios (see section 3.1.4). Looking at data compilations including data outside the Atlantic (Cullen, 2006; Quay et al., 2015; Xie et al., 2015) there is a lot of scatter in the data, which, like for the current Atlantic data set is probably related to mixing of different water masses and differing remineralisation ratios. However, for deep water (deeper than 2000 m, (Quay et al., 2015) their fig. 5) it is obvious there is no distinct kink outside the Atlantic for the deep ocean. For shallower water with lower PO_4 outside the Atlantic, it seems the data plots below the regressions observed for NADW and the surface NA (regressions 1, 2 and 3 in Fig. 3b), similar to the data from the SA (curve 8 in Fig. 3b) e.g. (Cullen, 2006; Xie et al., 2015).

In the Southern Ocean, Cd gets taken up in the surface ocean with a relatively high Cd:PO_4 uptake ratio (relation like regression 6 in Fig. 3b; Baars et al., 2014). Subsequent remineralisation in the subsurface water masses leads, on average, to a relatively high dissolved Cd/PO_4 ratio (compared to northern origin water) in the waters that eventually supply the low latitude oceans with nutrients (SAMW/AAIW). However, the shallower SAMW formed further north where the Cd concentrations are towards the lower end, is relatively depleted in Cd and has a lower Cd/PO_4 ratio compared to AAIW. Mixing between lower latitude surface water, SAMW and AAIW results in a convex line that becomes less convex in a northward direction. Alternatively, when only assessing the near surface SA, one finds a regression line that is much as steep as observed in the NA (north of ~15° N, see Fig. 3b, comparing line 1 and 2 to lower part of curve 8). The slope of this line in the subsurface

ocean has been interpreted as the Cd:PO_4 remineralisation ratio (Quay et al., 2015). However, as demonstrated in our model and observations, at least for the Atlantic Ocean this is not correct as we do not find evidence for a lower remineralisation ratio in the SA. The higher dissolved Cd/PO_4 ratio in the subsurface SA would actually imply a higher supply and remineralisation ratio in the SA compared to the NA. The slope of the regression between Cd and PO_4 is influenced by mixing and the presence of various water masses and, for example in the equatorial region, would lead to a steeper regression due to the shoaling of the nutricline (Fig. 2). For the Southern Ocean, the slope of regression is probably a more reliable approach to estimate the remineralisation ratio as the intermediate and deep waters all have a very similar Cd/PO_4 ratio (Baars et al., 2014) and there is no advection of water into the region with a different preformed ratio. Using mainly data from the NA and Southern Ocean, Quay et al. (2015) demonstrated, using slope-derived ratios and a simple box model, that differing remineralisation ratios with a lower ratio in the NA compared to the Southern Ocean (highest ratio) and the Pacific and Indian Ocean (intermediate ratios) can explain the main features of the global Cd-PO_4 relationship. Our interpretations are in agreement with Quay et al. (2015). However, we suggest a different mechanism where the availability of Cd in the surface ocean, rather than HNLC versus non-HNLC conditions could be the driving factor and argue against using the slope of the (surface) Cd-PO_4 relationship as representative of the local Cd:PO_4 remineralisation ratio.

Extrapolating to the Pacific and Indian Ocean where SAMW/AAIW also play an important role in the nutrient supply to surface waters, one would also expect a convex relationship, or a bi-linear relationship with a slope less steep than in the NA, especially where relatively ‘pure’ SAMW is present. As detailed, we expect this slope not to be representative of the remineralisation ratio. In the North Pacific Ocean, due to upwelling of Antarctic origin deep water, one would expect higher Cd availability and thus higher Cd:PO_4 remineralisation ratios

compared to the NA or even the SA if all available Cd is taken up in the surface. Currently meridional datasets of sufficient resolution are lacking to test this hypothesis, but new data that will soon emerge from the GEOTRACES programme should fill this void.

4 Conclusions

Our findings now conclusively demonstrate the Cd-PO_4 relationship in the Atlantic Ocean to be governed by a combination of hydrography and first-order biogeochemistry. The dominant driver is mixing between endmembers with different dissolved Cd/PO_4 concentration ratios that are set at the high latitudes. Simple remineralisation suffices to explain the remaining variability. We infer there is no fixed Cd:PO_4 uptake and remineralisation ratio, and suggest the observed ratios simply reflect the Cd availability in the surface ocean where higher Cd availability, notably in HNLC regions results in, or facilitates greater uptake.

The distribution of Cd and PO_4 is the result of the interplay of horizontal and vertical mixing processes, and biogenic particle export and remineralisation with a Cd:PO_4 ratio that is likely to be variable. Thus assuming a constant slope for the deep ocean Cd-PO_4 relationship, e.g. for the calculation of a Cd deficit based on PO_4 concentrations or the use of Cd:Ca in foraminifera as a paleotracer to infer past nutrient concentrations and ocean circulation (Boyle, 1988; Makou et al., 2010) needs to be done carefully with attention for the caveats. The slope for the deep ocean Cd-PO_4 relationship depends on the origin of the water masses, water mass mixing, remineralisation and the Cd:PO_4 ratio of the remineralised biomass. Each of these factors is likely to vary over time (De Baar et al., 1994), notably during the Last Glacial Maximum versus the modern ocean. Here it must be noted that the Cd:Ca in foraminifera as a paleotracer is mainly used as water mass tracer based on Cd (Marchitto and Broecker, 2006). However, also the inferred Cd concentration should be interpreted with caution as the Cd concentration in various water masses during formation and advection has likely varied over time for the same reasons as the Cd-PO_4 relationship.

498 It is currently uncertain if Cd plays an important nutritional role in primary production by
499 marine phytoplankton and this warrants further investigation. Nonetheless, the northern and
500 southern high latitude oceans are most sensitive to global change and notably changes in these
501 regions, will have ramifications for the supply of this potentially important nutrient metal as
502 well as other nutrients to the global ocean.

503 Acknowledgements

504 We express our gratitude to the captains and crew of the RV Pelagia and RRS James Cook
505 during the cruises. The nutrient data was provided by the NIOZ nutrient lab and the oxygen
506 data by Lesley Salt and Maaike Claus. Insightful comments by the editor and three reviewers
507 were much appreciated and substantially improved the manuscript. This work was supported
508 by the Netherlands Organization for Scientific Research (NWO) project grants 820.01.014
509 (GEOTRACES Netherlands-USA Joint Effort on Trace Metals in the Atlantic Ocean) and
510 839.08.410 (GEOTRACES, Global Change and Microbial Oceanography in the West Atlantic
511 Ocean) and the USA National Science Foundation (NSF) grants: OCE-0961579 and OCE-
512 1131387.

513 Author contributions

514 RM performed the sampling and analysis and led the data interpretations. SMACvH
515 performed the eOMP and contributed in the interpretations. HJWdB organised the cruises and
516 funding support and contributed in the interpretations. KWB led the analysis and contributed
517 in the interpretations.

518 References

519 Abe, K., Iseki, K., Okamura, K., Kiyomoto, Y., 2006. Lower Cd/P ratio in settling particles
520 than in surface seawater in the Okinawa Trough. J. Oceanogr. 62, 745-752.
521 Abouchami, W., Galer, S.J.G., de Baar, H.J.W., Alderkamp, A.C., Middag, R., Laan, P.,
522 Feldmann, H., Andreae, M.O., 2011. Modulation of the Southern Ocean cadmium isotope
523 signature by ocean circulation and primary productivity. Earth. Planet. Sci. Lett. 305, 83-91.
524 Anderson, L.A., Sarmiento, J.L., 1994. Redfield ratios of remineralization determined by
525 nutrient data analysis. Global Biogeochem. Cycles 8, 65-80.
526 Baars, O., Abouchami, W., Galer, S.J.G., Boye, M., Croot, P.L., 2014. Dissolved cadmium in
527 the Southern Ocean: Distribution, speciation, and relation to phosphate. Limnol. Oceanogr.
528 59, 385-399.
529 Boyle, E.A., 1988. CADMIUM: CHEMICAL TRACER OF DEEPWATER
530 PALEOCEANOGRAPHY. Paleoceanography 3, 471-489.
531 Boyle, E.A., Sclater, F., Edmond, J.M., 1976. On the marine geochemistry of cadmium.
532 Nature 263, 42-44.
533 Browning, T.J., Bouman, H.A., Henderson, G.M., Mather, T.A., Pyle, D.M., Schlosser, C.,
534 Woodward, E.M.S., Moore, C.M., 2014. Strong responses of Southern Ocean phytoplankton
535 communities to volcanic ash. Geophys. Res. Lett. 41, 2014GL059364.
536 Bruland, K.W., Knauer, G.A., Martin, J.H., 1978. Cadmium in Northeast Pacific waters.
537 Limnol. Oceanogr. 23, 618-625.
538 Bruland, K.W., Middag, R., Lohan, M.C., 2014. Controls of Trace Metals in Seawater, in:
539 Holland H.D, a.T.K.K. (Ed.), Treatise on Geochemistry 2nd edition, pp. 19-55.
540 Cid, A., Nakatsuka, S., Sohrin, Y., 2012. Stoichiometry among bioactive trace metals in the
541 Chukchi and Beaufort Seas. J. Oceanogr. 68, 985-1001.

542 Conway, T.M., John, S.G., 2015. Biogeochemical cycling of cadmium isotopes along a high-
543 resolution section through the North Atlantic Ocean. Geochim. Cosmochim. Acta 148, 269-
544 283.
545 Cullen, J.T., 2006. On the nonlinear relationship between dissolved cadmium and phosphate
546 in the modern global ocean: Could chronic iron limitation of phytoplankton growth cause
547 the kink? Limnol. Oceanogr. 51, 1369-1380.
548 Cullen, J.T., Lane, T.W., Morel, F.M.M., Sherrell, R.M., 1999. Modulation of cadmium
549 uptake in phytoplankton by seawater CO2 concentration. Nature 402, 165-167.
550 Danielsson, L.-G., Westerlund, S., 1983. Trace Metals in the Arctic Ocean, in: Wong, C.S.,
551 Boyle, E., Bruland, K.W., Burton, J.D., Goldberg, E.D. (Eds.), Trace Metals in Sea Water.
552 Springer US, Boston, MA, pp. 85-95.
553 De Baar, H.J.W., Dejong, J.T.M., Bakker, D.C.E., Loscher, B.M., Veth, C., Bathmann, U.,
554 Smetacek, V., 1995. Importance of Iron for Plankton Blooms and Carbon-Dioxide
555 Drawdown in the Southern-Ocean. Nature 373, 412-415.
556 De Baar, H.J.W., Saager, P.M., Nolting, R.F., Vandermeer, J., 1994. CADMIUM VERSUS
557 PHOSPHATE IN THE WORLD OCEAN. Mar. Chem. 46, 261-281.
558 de Souza, G.F., Slater, R.D., Dunne, J.P., Sarmiento, J.L., 2014. Deconvolving the controls on
559 the deep ocean's silicon stable isotope distribution. Earth. Planet. Sci. Lett. 398, 66-76.
560 Frew, R.D., 1995. Antarctic bottom water formation and the global cadmium to phosphorus
561 relationship. Geophys. Res. Lett. 22, 2349-2352.
562 Frew, R.D., Hunter, K.A., 1992. Influence of Southern Ocean waters on the cadmium-
563 phosphate properties of the global ocean. Nature 360, 144-146.
564 Horner, T.J., Lee, R.B.Y., Henderson, G.M., Rickaby, R.E.M., 2013. Nonspecific uptake and
565 homeostasis drive the oceanic cadmium cycle. Proceedings of the National Academy of
566 Sciences 110, 2500-2505.

Hupe, A., Karstensen, J., 2000. Redfield stoichiometry in Arabian Sea subsurface waters. Global Biogeochem. Cycles 14, 357-372.

Janssen, D.J., Conway, T.M., John, S.G., Christian, J.R., Kramer, D.I., Pedersen, T.F., Cullen, J.T., 2014. Undocumented water column sink for cadmium in open ocean oxygen-deficient zones. Proceedings of the National Academy of Sciences 111, 6888-6893.

Karstensen, J., Tomczak, M., 1998. Age determination of mixed water masses using CFC and oxygen data. Journal of Geophysical Research: Oceans 103, 18599-18609.

Klunder, M.B., Laan, P., Middag, R., De Baar, H.J.W., van Ooijen, J.C., 2011. Dissolved iron in the Southern Ocean (Atlantic sector). Deep-Sea Research Part Ii-Topical Studies in Oceanography 58, 2678-2694.

Lane, T.W., Morel, F.M.M., 2000. A biological function for cadmium in marine diatoms. Proceedings of the National Academy of Sciences of the United States of America 97, 4627-4631.

Mackas, D.L., Denman, K.L., Bennett, A.F., 1987. Least squares multiple tracer analysis of water mass composition. Journal of Geophysical Research: Oceans 92, 2907-2918.

Makou, M.C., Oppo, D.W., Curry, W.B., 2010. South Atlantic intermediate water mass geometry for the last glacial maximum from foraminiferal Cd/Ca. Paleoceanography 25, PA4101.

Marchitto, T.M., Broecker, W.S., 2006. Deep water mass geometry in the glacial Atlantic Ocean: A review of constraints from the paleonutrient proxy Cd/Ca. Geochem. Geophys. Geosyst. 7, n/a-n/a.

Martin, J., Bruland, K.W., Broenkow, W., 1976. Cadmium transport in the California current, in: Duce, H.L.W.a.R.A. (Ed.), Marine Pollutant Transfer Lexington Books, Toronto, pp. 84–159.

591 Mawji, E., Schlitzer, R., Dodas, E.M., Abadie, C., Abouchami, W., Anderson, R.F., Baars, O.,
592 Bakker, K., Baskaran, M., Bates, N.R., Bluhm, K., Bowie, A., Bown, J., Boye, M., Boyle,
593 E.A., Branellec, P., Bruland, K.W., Brzezinski, M.A., Bucciarelli, E., Buesseler, K., Butler,
594 E., Cai, P., Cardinal, D., Casciotti, K., Chaves, J., Cheng, H., Chever, F., Church, T.M.,
595 Colman, A.S., Conway, T.M., Croot, P.L., Cutter, G.A., de Baar, H.J.W., de Souza, G.F.,
596 Dehairs, F., Deng, F., Dieu, H.T., Dulaquais, G., Echegoyen-Sanz, Y., Lawrence Edwards,
597 R., Fahrbach, E., Fitzsimmons, J., Fleisher, M., Frank, M., Friedrich, J., Fripiat, F., Galer,
598 S.J.G., Gamo, T., Solsona, E.G., Gerringa, L.J.A., Godoy, J.M., Gonzalez, S., Grossteffan,
599 E., Hatta, M., Hayes, C.T., Heller, M.I., Henderson, G., Huang, K.-F., Jeandel, C., Jenkins,
600 W.J., John, S., Kenna, T.C., Klunder, M., Kretschmer, S., Kumamoto, Y., Laan, P., Labatut,
601 M., Lacan, F., Lam, P.J., Lannuzel, D., le Moigne, F., Lechtenfeld, O.J., Lohan, M.C., Lu,
602 Y., Masqué, P., McClain, C.R., Measures, C., Middag, R., Moffett, J., Navidad, A.,
603 Nishioka, J., Noble, A., Obata, H., Ohnemus, D.C., Owens, S., Planchon, F., Pradoux, C.,
604 Puigcorbé, V., Quay, P., Radic, A., Rehkämper, M., Remenyi, T., Rijkenberg, M.J.A.,
605 Rintoul, S., Robinson, L.F., Roeske, T., Rosenberg, M., van der Loeff, M.R., Ryabenko, E.,
606 Saito, M.A., Roshan, S., Salt, L., Sarthou, G., Schauer, U., Scott, P., Sedwick, P.N., Sha, L.,
607 Shiller, A.M., Sigman, D.M., Smethie, W., Smith, G.J., Sohrin, Y., Speich, S., Stichel, T.,
608 Stutsman, J., Swift, J.H., Tagliabue, A., Thomas, A., Tsunogai, U., Twining, B.S., van
609 Aken, H.M., van Heuven, S., van Ooijen, J., van Weerlee, E., Venchiarutti, C., Voelker,
610 A.H.L., Wake, B., Warner, M.J., Woodward, E.M.S., Wu, J., Wyatt, N., Yoshikawa, H.,
611 Zheng, X.-Y., Xue, Z., Zieringer, M., Zimmer, L.A., 2015. The GEOTRACES Intermediate
612 Data Product 2014. Mar. Chem. 177, Part 1, 1-8.
613 Middag, R., de Baar, H.J.W., Klunder, M.B., Laan, P., 2013. Fluxes of dissolved aluminum
614 and manganese to the Weddell Sea and indications for manganese co-limitation. Limnol.
615 Oceanogr. 58, 287-300.

Middag, R., Séférian, R., Conway, T.M., John, S.G., Bruland, K.W., de Baar, H.J.W., 2015. Intercomparison of dissolved trace elements at the Bermuda Atlantic Time Series station. Mar. Chem. 177, Part 3, 476-489.

Morel, F.M.M., 2013. The oceanic cadmium cycle: Biological mistake or utilization? Proceedings of the National Academy of Sciences of the United States of America 110, E1877-E1877.

Price, N.M., Morel, F.M.M., 1990. Cadmium and Cobalt substitution for zinc in a marine diatom. Nature 344, 658-660.

Quay, P., Cullen, J., Landing, W., Morton, P., 2015. Processes controlling the distributions of Cd and PO4 in the ocean. Global Biogeochem. Cycles 29, 830-841.

Rijkenberg, M.J.A., de Baar, H.J.W., Bakker, K., Gerringa, L.J.A., Keijzer, E., Laan, M., Laan, P., Middag, R., Ober, S., van Ooijen, J., Ossebaar, S., van Weerlee, E.M., Smit, M.G., 2015. “PRISTINE”, a new high volume sampler for ultraclean sampling of trace metals and isotopes. Mar. Chem. 177, Part 3, 501-509.

Rijkenberg, M.J.A., Middag, R., Laan, P., Gerringa, L.J.A., van Aken, H.M., Schoemann, V., de Jong, J.T.M., de Baar, H.J.W., 2014. The Distribution of Dissolved Iron in the West Atlantic Ocean. Plos One 9.

Roshan, S., Wu, J., 2015. Cadmium regeneration within the North Atlantic. Global Biogeochem. Cycles 29, 2082-2094.

Rudels, B., Muench, R.D., Gunn, J., Schauer, U., Friedrich, H.J., 2000. Evolution of the Arctic Ocean boundary current north of the Siberian shelves. J. Mar. Syst. 25, 77-99.

Sarmiento, J.L., Gruber, N., Brzezinski, M.A., Dunne, J.P., 2004. High-latitude controls of thermocline nutrients and low latitude biological productivity. Nature 427, 56-60.

Schlitzer, R., 2016. Ocean Data View, https://odv.awi.de.

640 Stramma, L., England, M.H., 1999. On the water masses and mean circulation of the South
641 Atlantic Ocean. Journal of Geophysical Research-Oceans 104, 20863-20883.
642 Sunda, W.G., Huntsman, S.A., 2000. Effect of Zn, Mn, and Fe on Cd accumulation in
643 phytoplankton: Implications for oceanic Cd cycling. Limnol. Oceanogr. 45, 1501-1516.
644 Tomczak, M., 1981. A multi-parameter extension of temperature/salinity diagram techniques
645 for the analysis of non-isopycnal mixing. Prog. Oceanogr. 10, 147-171.
646 Twining, B.S., Baines, S.B., 2013. The Trace Metal Composition of Marine Phytoplankton.
647 Annual Review of Marine Science 5, 191-215.
648 Van Aken, H.M., 2007. The Oceanic Thermohaline Circulation: An Introduction. Springer
649 Science + Business Media, New York, USA.
650 Vance, D., Little, S.H., de Souza, G.F., Khatiwala, S., Lohan, M.C., Middag, R., 2017. Silicon
651 and zinc biogeochemical cycles coupled through the Southern Ocean. Nature Geosci 10,
652 202-206.
653 Wyatt, N.J., Milne, A., Woodward, E.M.S., Rees, A.P., Browning, T.J., Bouman, H.A.,
654 Worsfold, P.J., Lohan, M.C., 2014. Biogeochemical cycling of dissolved zinc along the
655 GEOTRACES South Atlantic transect GA10 at 40°S. Global Biogeochem. Cycles 28, 44-
656 56.
657 Xie, R.C., Galer, S.J.G., Abouchami, W., Rijkenberg, M.J.A., de Baar, H.J.W., De Jong, J.,
658 Andreae, M.O., 2017. Non-Rayleigh control of upper-ocean Cd isotope fractionation in the
659 western South Atlantic. Earth. Planet. Sci. Lett. 471, 94-103.
660 Xie, R.C., Galer, S.J.G., Abouchami, W., Rijkenberg, M.J.A., De Jong, J., de Baar, H.J.W.,
661 Andreae, M.O., 2015. The cadmium–phosphate relationship in the western South Atlantic
662 — The importance of mode and intermediate waters on the global systematics. Mar. Chem.
663 177, Part 1, 110-123.

Xu, Y., Tang, D., Shaked, Y., Morel, F.M.M., 2007. Zinc, cadmium, and cobalt interreplacement and relative use efficiencies in the coccolithophore Emiliania huxleyi. Limnol. Oceanogr. 52, 2294-2305.

669 Figure 1 Dissolved concentrations of Cd versus PO_4 from the GEOTRACES 2017
670 Intermediate Data product

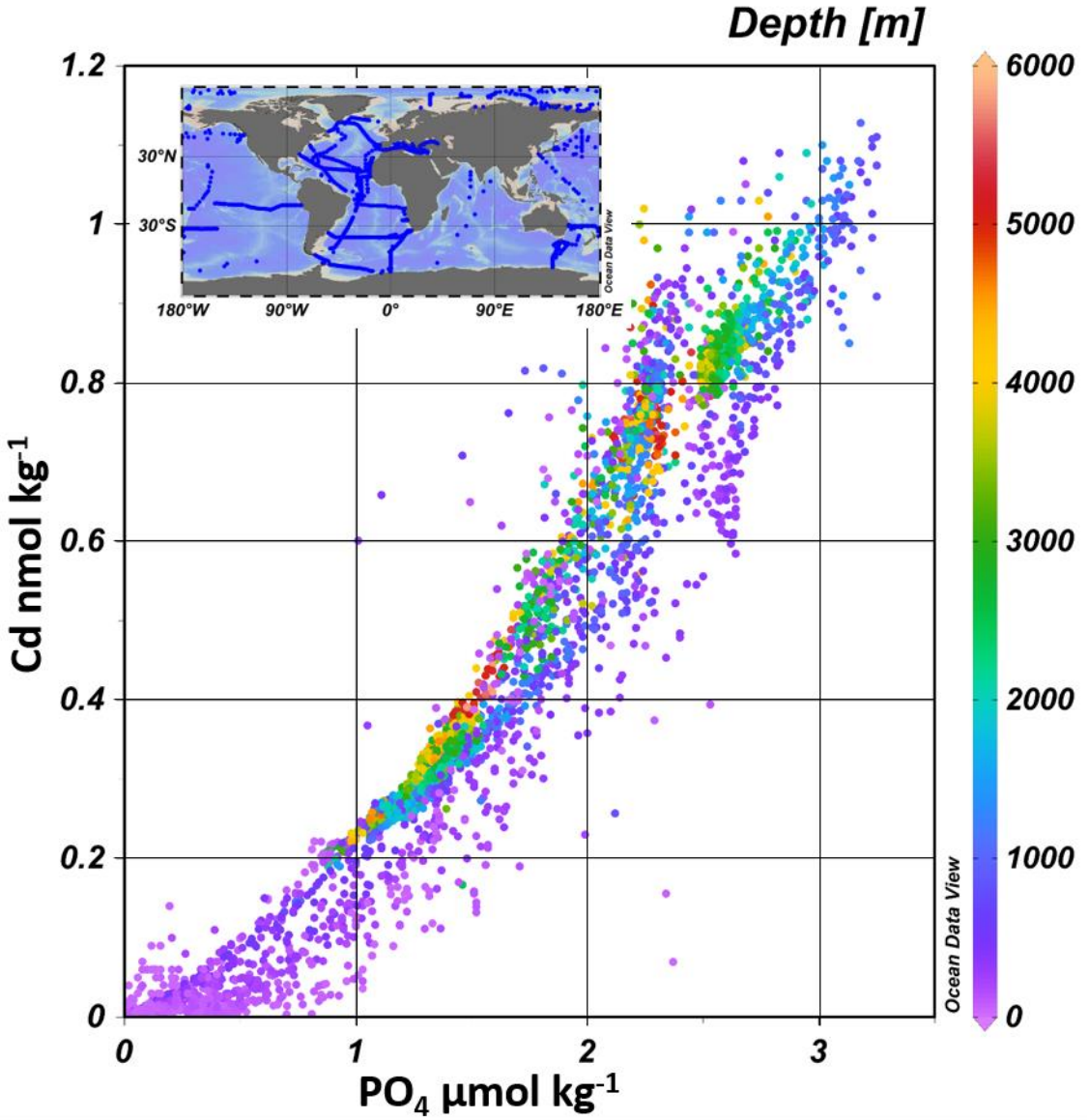

671

672 The concentrations of dissolved Cd (pmol kg^{-1}) versus dissolved PO_4 (µmol kg^{-1}). This is all
673 data that was included in the 2017 GEOTRACES Intermediate Data Product. We opted to
674 show this data, as the accuracy has been verified for these data (Mawji et al., 2015; Schlitzer,
675 2016).

676

677 Figure 2 Dissolved Cd and PO_4 concentrations along GEOTRACES transect GA02.
678

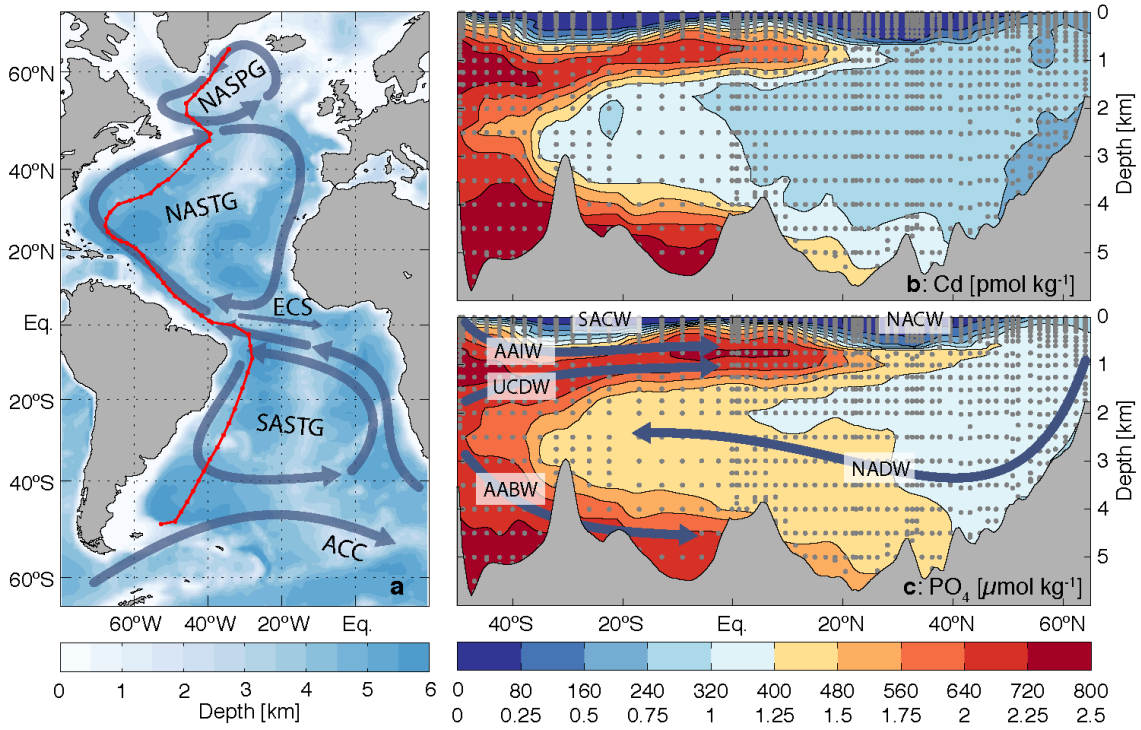

679

680 **a** The GEOTRACES transect GA02 (red line) with 60 stations in the West Atlantic with the
681 main surface hydrography (North Atlantic Sub-Polar Gyre, North Atlantic Sub-Tropical Gyre,
682 Equatorial Current System, South Atlantic Sub-Tropical Gyre and Antarctic Circumpolar
683 Current).

684 **b** Dissolved Cd in colour scale (0-800 pmol kg^{-1}) along the transect.

685 **c** Dissolved PO_4 in colour scale (0-2.5 μmol kg^{-1}) along the transect with the main water
686 masses and ocean pathways (AntArctic Bottom Water, Antarctic Intermediate Water, North
687 Atlantic Central Water, North Atlantic Deep Water, South Atlantic Central Water and Upper
688 Circumpolar Deep Water).

689

690

Figure 3 Dissolved Cd [pmol kg^{-1}] versus dissolved PO_4 [µmol kg^{-1}]

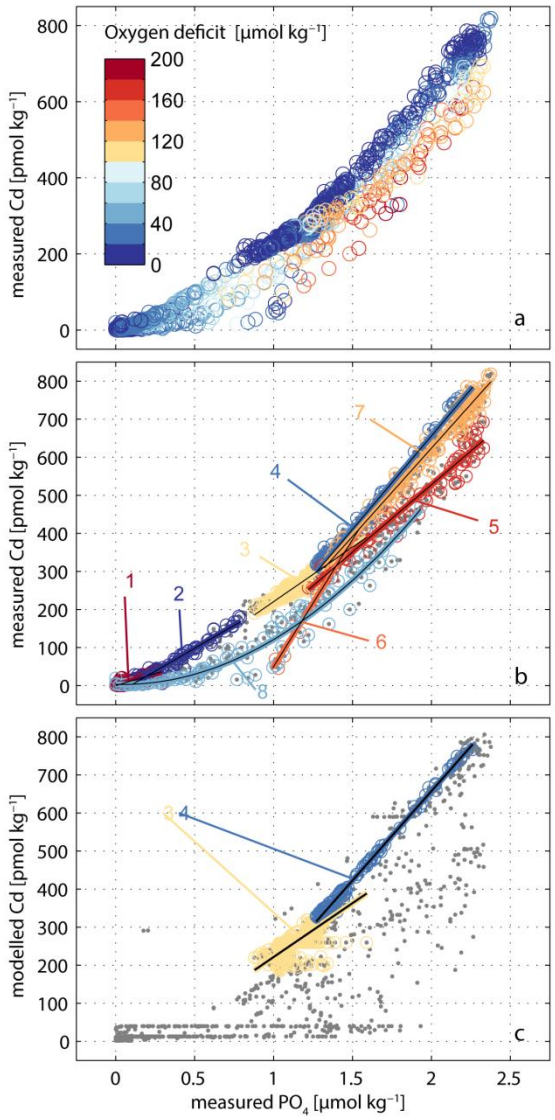

a Measured Cd versus measured PO_4 with the oxygen deficit in colour scale. Note that the samples with high oxygen deficit have a comparatively low Cd/PO_4 ratio.

b Measured Cd versus measured PO_4 with 8 regressions. These are, respectively 1: NASTMW, 2: NASPMW, 3: NADW, 4: NADW-AABW mixing, 5: NADW-AAIW-UCDW mixing, 6: SASPMW-AAIW mixing, 7: AAIW-UCDW-AABW mixing, 8: SASTMW-AAIW- SASPMW mixing. See Table S6 for details. Coloured circles around grey data points indicate to which water mass or mixing line the data point belongs.

c Modelled Cd (mixing model without accounting for remineralisation) with predetermined Cd-endmembers versus measured PO_4. Regressions 3 and 4 are the same as in Fig. 3b to illustrate that the 'mixing only' model reproduces the kink at around PO_4 = ~1.3 [µmol kg^{-1}] in the Cd-PO_4 relationship. Yellow circles around grey data points indicate data points that are considered NADW, blue circles indicate the NADW-AABW mixture.

Figure 4 Modelled Cd versus measured Cd with oxygen deficit in colour scale.

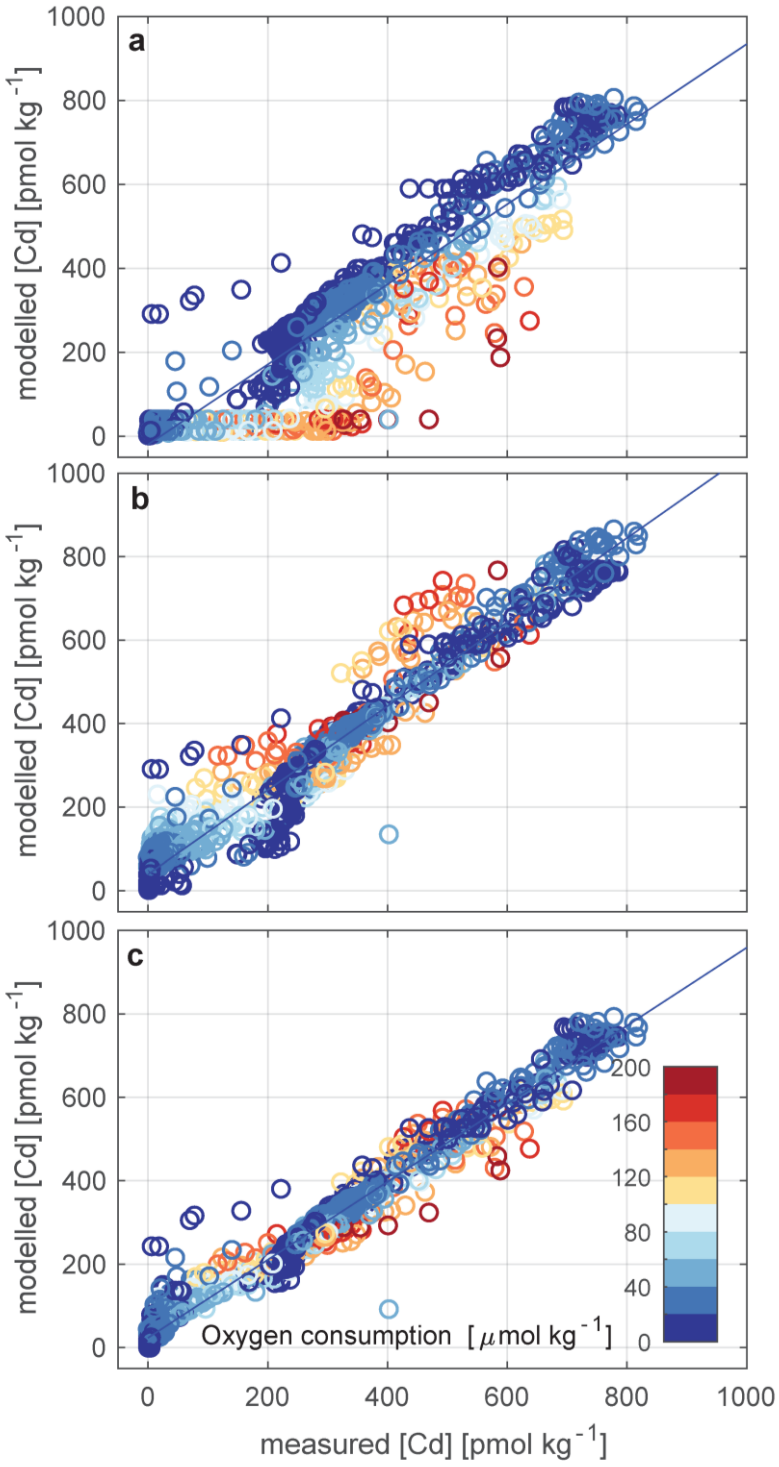

a Modelled Cd versus measured Cd for the model with predetermined Cd-endmembers. Modelled = 0.95 (±0.02) * measured -20 (±7); R^2=0.86; rmse= 80 pmol kg^{-1}

b Model with predetermined Cd-endmembers and an invariable Cd:O_2 ratio of 2 pmol/µmol. Modelled = 1.00 (+-0.01) * measured + 40 (+-4); R^2=0.95; rmse= 48 pmol kg^{-1}

c Model with optimised Cd-endmembers and an optimised Cd:O_2 ratio of 1.25±0.03 pmol/umol Modelled = 0.94 (+-0.01) * measured + 24 (+-3); R^2=0.98; rmse= 32 pmol kg^{-1}

718 Figure 5 The dissolved Cd/PO_4 ratio and the Cd residuals (measured – modelled) along the
719 transect
720

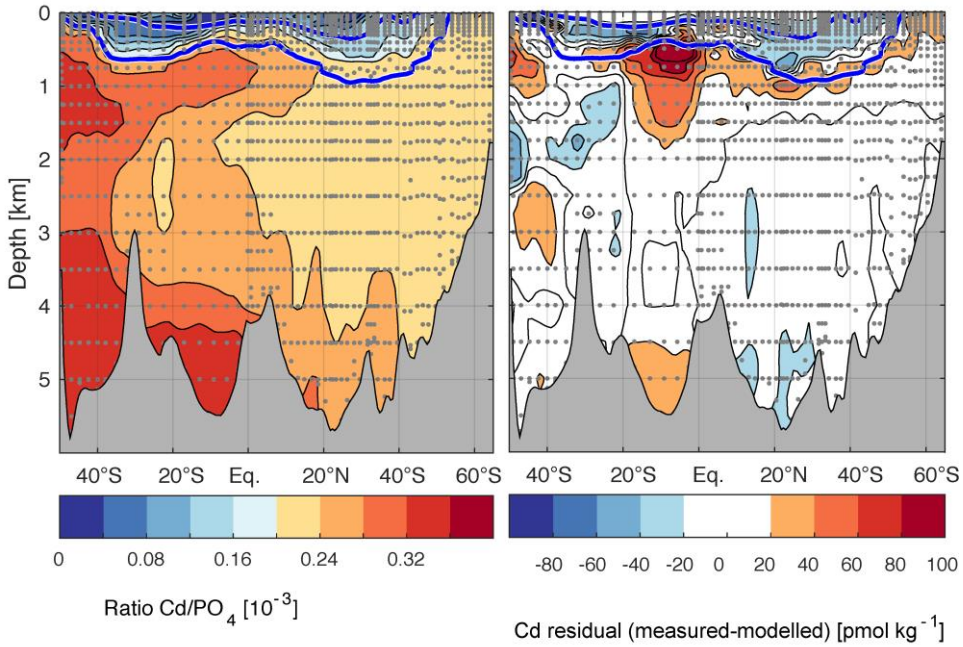

721
722 **a** The dissolved Cd/PO_4 ratio (from measurements) along the transect showing the higher
723 Cd/PO_4 ratio in Antarctic origin waters. The blue lines denote the 8 °C and 18 °C isobars
724 where 8°C serves to illustrate the deep end of the thermocline. The Cd/PO_4 ratio at the deep
725 end of the thermocline is in the 0.20 – 0.24 nmol/µmol range except except for the equatorial
726 region were the ratio is slightly higher (up to 0.27 nmol/µmol).
727 **b** The difference between the measured Cd concentrations and the modelled Cd
728 concentrations with the optimised eOMP model in pmol kg^{-1}. The average absolute relative
729 deviation is 4.8% in water deeper than 400m and a Cd concentration greater than 100 pmol
730 kg^{-1} (higher relative deviations are observed in the surface ocean, inherently related to the
731 depleted surface Cd concentrations).
732

733 Figure 6 The fraction remineralised Cd over the water column

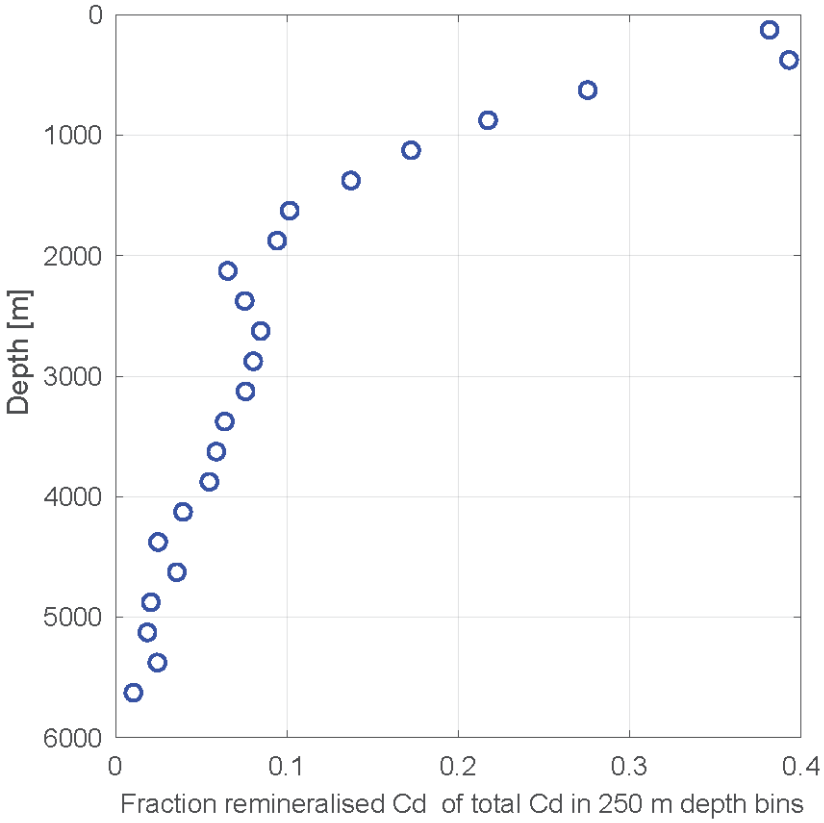

734

735 The vertical profile of the fraction remineralised Cd (inferred from eOMP-derived oxygen
736 consumption and the O_2/Cd remineralisation ratio) of total (i.e., measured) Cd for 250 m
737 depth ranges. For every 250 m depth interval, the average fraction remineralised Cd (inferred
738 from eOMP-derived oxygen consumption and the O_2/Cd remineralisation ratio) was
739 calculated. For this calculation, concentrations of Cd in the observed depth bin are summed
740 and divided by the summed remineralised Cd in the same depth bin (i.e. the figure represents
741 the transect average) rather than using the mean of the 'spot-ratios' as done previously (Rohan
742 and Wu, 2015). In the presence of near-zero values (i.e., in surface waters), ratios and
743 averages thereof become meaningless. Our method of summing before dividing does not have
744 this drawback, making it possible to also calculate a value for the surface ocean.

Supplementary material

The relationship between cadmium and phosphate in the Atlantic ocean unravelled

Rob Middag, Steven M.A.C. van Heuven, Ken W. Bruland, Hein J.W. de Baar

Methodological details

Cadmium

Samples were filtered (0.2 µm) and acidified (0.024 M Baseline® hydrochloric acid) shipboard in acid cleaned low density polyethylene bottles and analysed on shore as described previously (Middag et al., 2015). The precision based on replicate analysis (n=13) of reference seawater was ~1.4 % at 978 pmol kg^{-1}, 2.1 % at 265 pmol kg^{-1}, and around 20% at levels < 5 pmol kg^{-1}. Of the 1434 samples analysed for Cd, there were 7 rejected as outliers (see Middag et al., 2011 for criteria) and not used in the dataset. Another 69 samples were below the detection limit (< 1pmol kg^{-1}) and these values were flagged, but kept in the dataset. The absolute values of these 69 samples are not used in any direct interpretation, but the data points were used in the plots and regressions where they represent the lowest range of the Cd distribution in the ocean.

Nutrients

Concentrations of oxygen and nutrients were measured in general accordance with GO-SHIP protocol (Hood et al., 2010). The oxygen sensor was calibrated against discrete water samples, analysed on board. Samples for nutrients (PO_4, nitrate, nitrite and silicate) were collected unfiltered in high density polyethylene sample bottles which were rinsed three times with sample water as described previously (Rijkenberg et al., 2015). A sterilised natural Reference Nutrient Sample (Kanso, Lot code AX) containing known concentrations of nutrients in Pacific Ocean water, was analysed in triplicate every run. The precision was around 0.6% of the average value and there was no significant difference between the shipboard measured values of Kanso and the consensus values (Rijkenberg et al., 2015). Specifically for PO_4, the detection limit is 0.01 µmol kg^{-1} with a precision of around 10% near the detection limit. The deepest sample analysed for a station of 24 samples, was kept and re-analysed within the next run of the next station of 24 samples as verification for variability between runs.

eOMP water type definitions

The water type characteristics (Table S1) are not necessarily linked (e.g., not based on a single, coherent sample) or related mathematically. They were chosen per parameter on the basis of the extremes of property-property plots (e.g. S-T plots) of the dataset of this cruise or of end-of-section values. Obviously, the chosen values will closely reflect at least a few samples constituting the (inferred) core of the water mass. That is, all water types are represented in rather pure form at some point along our section. Water type definitions to some extent are subjective, and tailored to an intended application. The point of the OMP in this manuscript is to unravel mixing processes from biogeochemical processes in the distribution of dissolved Cd. The extremes of the observations are represented in the water type definitions, so that every sample along our section attains an acceptable eOMP solution. Restrictions were imposed on the presumed spatial extent of water types in order to limit the number of types to be considered to contribute to a sample, so as not to underconstrain the eOMP solution (Table S2).

eOMP model robustness and uncertainty

To obtain an estimate of the robustness of the eOMP result, each sample is analysed one thousand times following the eOMP procedure outlined above in the main text, while each time slightly varying (i) the characteristics of the endmember water types and (ii) the remineralisation ratio, all by sampling from a normal distribution of width around the nominal definition. These widths are generally broader for shallower water types, and narrow for the large bottom waters (Table S1). These subjective uncertainties may be considered coarse estimates of the temporal variability of the real-world water masses around their nominal values (or, in the case of water masses consisting of two water types, deviations from their nominal mixing lines; see Tomczak, 1999). For the remineralisation ratios, we use double the uncertainties reported by Anderson and Sarmiento 1994 (i.e., $\Delta P:\Delta N:\Delta O2$ = 1:16±1:-170±10) as these ratios are known to be variable.

For each sample one thousand estimates of the most likely constitution are thus obtained given one thousand slightly varying sets of endmember water types and remineralisation ratios. For each sample, for each water contributing water type, the uncertainty is defined as the standard deviation of the one thousand MonteCarlo estimates. Water type fractions are summed into water mass fractions for those water masses that are defined as to consist of 2 water types (see Tomczak, 1999). Uncertainties for water mass fractions are obtained as the root of the sum of squares of uncertainties of the constituent water types. Robustness of the results is here expressed, for each water mass, as the ratio of (i) the number or samples for which the standard deviation of one thousand contribution estimates does not exceed 20% over (ii) the number of samples for which the mean of 1000 contribution estimates is at least 20%. That is, robustness is indicated by the fraction of samples that contain an appreciable amount of a water type and for which that amount is less uncertain than ±20% (Table S3). The uncertainty analysis demonstrates that the nominal result is not merely a statistical fluke but that, independent of the exact setup or water type definitions of the eOMP, the result is robust. The eOMP results of the near-surface samples included in this study should be judged with some caution, due to exchange with the atmosphere (oxygen, heat, and salinity through evaporation), which may invalidate assumptions of the eOMP analysis to unknown degree. Note that the inclusion of any invalid samples in the eOMP does not compromise the validity of results obtained for other samples, because every sample is analysed independently of all others.

Obtaining remineralisation ratios and optimum Cd endmembers

With water mass fractions and remineralisation obtained by the eOMP procedure, estimates are subsequently obtained of (i) optimal Cd values for each water type and (ii) the $\Delta Cd:\Delta O_2$ remineralisation ratio, via inversion of the system as follows:

$$Cd_{meas} = X \bullet E + D \bullet R \qquad \text{(Eq. 1)}$$

i.e.,

$$[E\ R] = [X\ D]^{-1} \bullet Cd_{meas} \qquad \text{(Eq. 2)}$$

where X represents the vector of water type contributions (as obtained earlier by eOMP), E is the vector of optimal Cd endmembers to be inferred, D represents the amount of oxygen utilised for remineralisation of organic matter (also obtained earlier from from eOMP), and R represents the remineralisation ratio $\Delta Cd:\Delta O_2$ (to be inferred). A nonnegative solver is employed, to prevent inferrence of negative endmember Cd concentration. This procedure is followed for each of the 1000 MonteCarlo runs and standard deviations of the results is reported as the uncertainty of the Cd endmembers and Cd:-O_2 ratios (section 3.3 and Table S4). These uncertainties thus include both the uncertainties in the remineralisation ratios (i.e., $\Delta P:\Delta N:\Delta O2$ = 1:16±1:-170±10) and the variations in the eOMP setup (Table S1).

WATERMASS	WATERTYPE	Theta [°C]	Salinity	NO_3 [µmol kg^{-1}]	Si [µmol kg^{-1}]	O_2 [µmol kg^{-1}]
AABW	AABW	-0.10 +- 0.02	34.66 +- 0.01	33.0 +- 0.8	125.0 +- 4.0	210 +- 4
NADW	DSOW	1.50 +- 0.02	34.870 +- 0.002	13.0 +- 0.8	9.0 +- 8.0	300 +- 3
	LSW	3.40 +- 0.07	34.89 +- 0.01	16.0 +- 0.5	10.0 +- 1.0	280 +- 5
UCDW	UCDW	2.60 +- 0.10	34.75 +- 0.05	35.0 +- 0.2	65.0 +- 5.0	170 +- 5
AAIW	AAIW	3.80 +- 0.10	34.05 +- 0.03	25.0 +- 1.0	13.0 +- 2.0	270 +- 7
SACW	SASPMW	10.00 +- 0.20	34.80 +- 0.05	12.0 +- 2.0	4.0 +- 3.0	285 +- 10
	SASTMW	18.00 +- 0.20	36.00 +- 0.05	1.0 +- 0.2	2.0 +- 0.5	240 +- 10
NACW	NASPMW	8.00 +- 0.20	34.95 +- 0.05	10.0 +- 2.0	6.0 +- 3.0	290 +- 10
	NASTMW	18.00 +- 0.20	36.55 +- 0.05	0.1 +- 0.2	1.0 +- 0.5	235 +- 10
ESW	ESW-1	29.00 +- 3.00	33.00 +- 0.30	0.3 +- 0.1	1.0 +- 1.0	193 +- 5
	ESW-2	28.00 +- 3.00	37.50 +- 0.30	0.2 +- 0.1	0.5 +- 1.0	202 +- 5

Table S1. Water mass and water type definitions (and the uncertainties used in the MonteCarlo procedure) for salinity, temperature, O_2, Si and NO_3 for the 11 water types as used in the extended optimum multiparameter (eOMP) analysis.

Abbreviations: AntArctic Bottom Water, North Atlantic Deep Water, Denmark Strait Overflow Water, Labrador Sea Water, Upper Circumpolar Deep Water, AntArctic Intermediate Water, South Atlantic Central Water, South Atlantic Sub-Polar Mode Water, South Atlantic Sub-Tropical Mode Water, North Atlantic Central Water, North Atlantic Sub-Polar Mode Water, North Atlantic Sub- Tropical Mode Water, Equatorial Surface water. (NB The South Atlantic Sub-Polar Mode Water here is similar to the SubAntarctic Mode Water (SAMW) in some of the preceding literature.)

WATERTYPE	Range latitude °N	Depth range [m]	Range Theta [°C]
AABW	-90 - < -45	0 - bottom	-3.0 - 4.0
	-45 - < 0	700 - bottom	-3.0 - 4.0
	0 - 60	2000 - bottom	-3.0 - 4.0
DSOW	-60 - < 70	1000 - bottom	-3.0 - 10.0
	30 - < 70	0 - bottom	-3.0 - 10.0
LSW	-60 - < 70	500 - bottom	-3.0 - 10.0
	0 - < 70	0 - bottom	-3.0 - 10.0
UCDW	-90 - < -40	0 - 2500	0.0 - 99.0
	-90 - < 20	500 - 2500	0.0 - 99.0
AAIW	-65 - < -25	0 - 2000	0.0 - 10.0
SASPMW	-65 - < -20	0 - 1200	5.0 - 17.0
SASTMW	-65 - < -20	0 - 1200	8.0 - 50.0
NASPMW	0 - < 65	0 - 1500	3.0 - 20.0
NASTMW	0 - < 65	0 - 1500	7.0 - 50.0
ESW-1	-30 < 35	0 - 500	15.0 - 50.0
ESW-2	-40 < 40	0 - 500	15.0 - 50.0

Table S2. Restrictions imposed on the presumed spatial extent of water types in order to limit the number of types to be considered to contribute to a sample.

	Robustness (%)			
Water Mass	1σ 1σ	2σ 1σ	1σ 2σ	2σ 2σ
Antarctic Bottom Water	100	100	100	100
North Atlantic Deep Water	83	81	74	74
Upper Circumpolar Deep	100	100	97	94
Antarctic Intermediate Water	92	86	88	84
South Atlantic Central Water	81	77	62	60
North Atlantic Central Water	95	92	64	62
Equatorial Surface Water	100	100	56	54

Table S3. Robustness of eOMp results as discussed in text. The different columns are for different uncertainty scenarios were 1σ 1σ uses the uncertainty on the remineralisation ratio as reported by Anderson and Sarmiento 1994 ($\Delta P:\Delta N:\Delta O_2$ = 1:16±1:-170±10) and the uncertainty ranges for the eOMP endmembers as reported in Table S1. The 2σ 1σ is as used in the manuscript, double the uncertainty on the remineralisation ratio and the range on the eOMP endmembers as reported in Table S1. The 1σ 2σ scenario has the uncertainty on the remineralisation ratio as reported by Anderson and Sarmiento 1994 and double the uncertainty ranges for the eOMP endmembers, whereas the final scenario (2σ 2σ) has double the uncertainty ranges on both the remineralisation ratio and the eOMP endmembers. For example for scenario 2σ 1σ as used in the manuscript, for 19 % of those samples that nominally contain >20% NADW that fraction is easily perturbed. For the remaining 81% of the samples that nominally contain >20% NADW the fraction is insensitive to our perturbation experiment (their standard deviation < 20%), these are likely the samples in the core of the water mass. Increasing the uncertainty mainly influences the (near) surface waters as these have larger uncertainty ranges and are more affected by remineralisation.

	Cd endmembers				
WATERTYPE	Predefined	1σ 1σ	2σ 1σ	1σ 2σ	2σ 2σ
AABW	800	783 ± 2	784 ± 2	786 ± 2	787 ± 3
DSOW	220	190 ± 2	190 ± 2	199 ± 2	200 ± 4
LSW	260	238± 1	238± 1	236± 1	237± 2
UCDW	900	823 ± 7	813 ± 7	811 ± 7	789 ± 11
AAIW	590	527 ± 4	528 ± 4	529 ± 4	535 ± 6
SASPMW	40	70 ± 4	73 ± 5	70 ± 5	86 ± 8
SASTMW	40	0	0	0	0
NASPMW	13	132 ± 2	133 ± 3	128 ± 3	139 ± 5
NASTMW	13	0	0	0	0
ESW-1	2	0	0	0	0
ESW-2	2	0	0	0	0
Remineralisation ratio Cd:-O_2 (x10^{-3})	2:1	1.27 ± 0.02 :1	1.25 ± 0.03 :1	1.26 ± 0.03 :1	1.13 ± 0.05 :1

Table S4. The predefined and optimised values of Cd (in units of pmol kg^{-1}) for the 11 water types used in the eOMP. Additionally the unitless Cd:-O_2 (x10^{-3}) is given (predefined and inferred from eOMP). The different uncertainty scenarios as in Table S3. The endmember solutions remain largely consistent under all scenarios. The inferred remineralisation ratio remains consistent, except in the most extreme uncertainty scenario (2σ 2σ).

	PO_4 endmembers				
WATERTYPE	Predefined	1σ 1σ	2σ 1σ	1σ 2σ	2σ 2σ
AABW	2.30	2.30 ± 0.01	2.30 ± 0.01	2.31 ± 0.01	2.31 ± 0.01
DSOW	0.90	0.93 ± 0.01	0.93 ± 0.01	0.95 ± 0.01	0.94 ± 0.01
LSW	1.10	1.06 ± 0.01	1.06 ± 0.01	1.05 ± 0.01	1.06 ± 0.01
UCDW	2.35	2.35 ± 0.01	2.35 ± 0.01	2.38 ± 0.01	2.36 ± 0.01
AAIW	1.90	1.78 ± 0.01	1.78 ± 0.01	1.79 ± 0.01	1.82 ± 0.01
SASPMW	1.00	0.73 ±0.01	0.74 ±0.01	0.76 ±0.01	0.82 ±0.01
SASTMW	0.10	0.01 ± 0.01	0.01 ± 0.01	0.01 ± 0.01	0.02 ± 0.01
NASPMW	1.00	0.59 ± 0.01	0.60 ± 0.01	0.61 ± 0.01	0.67 ± 0.01
NASTMW	0.10	0	0	0	0
ESW-1	0.03	0	0	0	0
ESW-2	0.1	0	0	0	0
Remineralisation ratio -O_2: PO_4	170:1	169 ± 2 :1	173 ± 2 :1	178 ± 3 :1	201 ± 7 :1

Table S5. The predefined and optimised values of PO_4 (in units of µmol kg^{-1}) for the 11 water types used in the eOMP. Additionally the unitless -O_2: PO_4 is given (predefined and inferred from eOMP). The different uncertainty scenarios as in Table S3. The endmember solutions remain largely consistent under all scenarios. The inferred remineralisation ratio remains consistent, except in the most extreme uncertainty scenario (2σ 2σ).

regression	equation	R^2	Data selection
1	Cd = 126 * PO_4 + 0.2	0.81	LAT>10°N & PO_4<0.3
2	Cd = 241 * PO_4 -22	0.94	LAT>40°N & PO_4>0.1 & PO_4<0.8
3	Cd = 287 * PO_4 - 66	0.87	LAT>0°N & NADW>75%
4	Cd = 491 * PO_4 - 325	0.99	LAT>-20°N & AABW>15%
5	Cd = 354 * PO_4 - 180	0.95	LAT>-10°N & LAT<20ºN & DEP>500 & DEP<1600
6	Cd = 667 * PO_4 - 616	0.98	LAT<-40°N & SAMW>30% & PO_4<1.
7	Cd = 463 * PO_4 - 303	0.98	LAT<-15°N & SACW<30% & ESW<30%
8	Cd = 129 * $(PO_4)^2$ – 11 * PO_4 + 3.5	0.95	SACW>75%

Table S6. The equations and data selections used for the 8 regressions in Fig 3b. The Cd concentrations are given in pmol kg^{-1} and PO_4 concentrations in µmol kg^{-1}. The criteria in the righthand column are solely used to assign the Cd and PO_4 data to separate regressions.

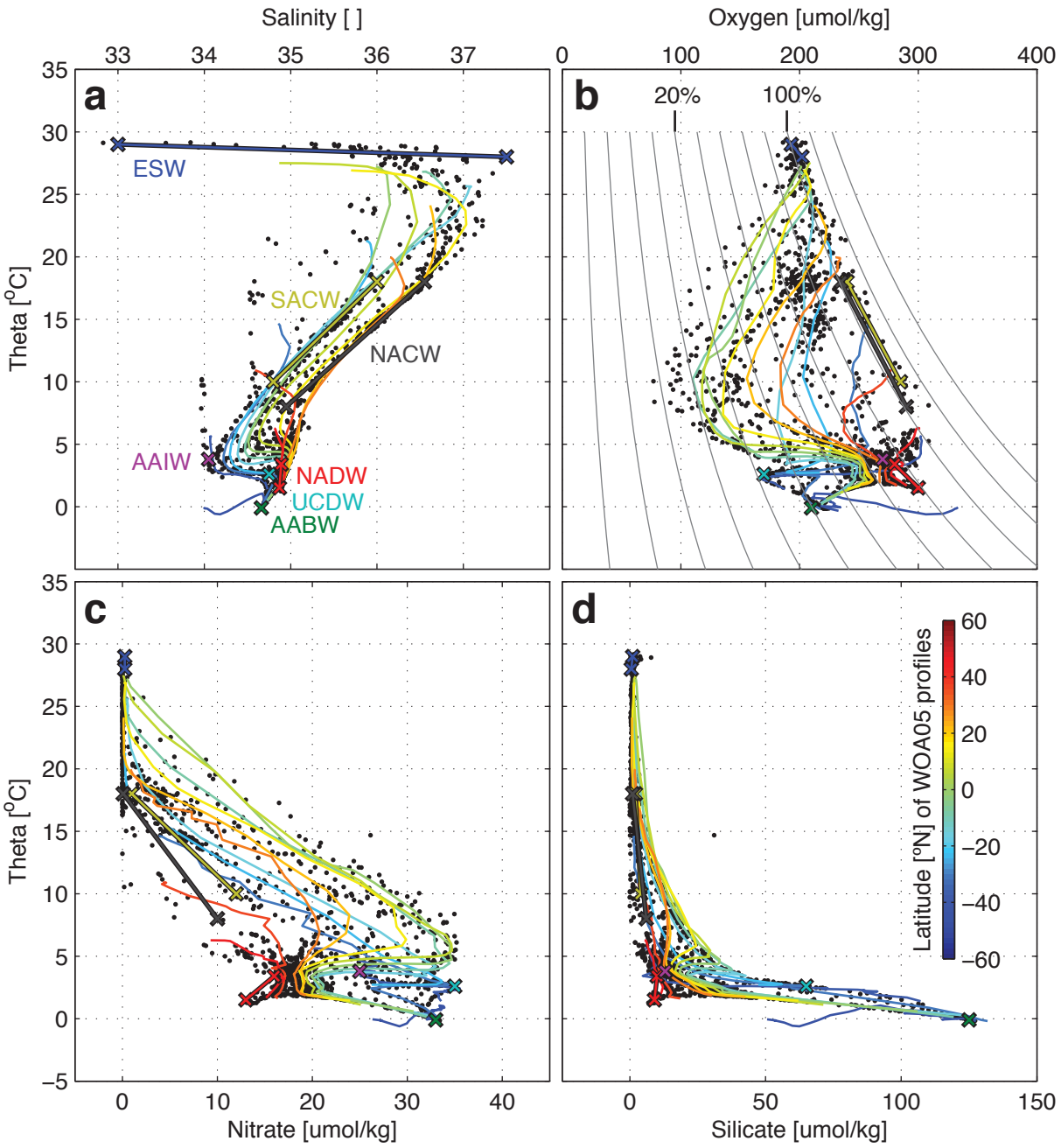

Figure S1. Property-property plots illustrating the hydrographical and chemical characteristics of the samples used in this study. To aid interpretation, overlaid as coloured lines are profiles taken from the World Ocean Atlas 2005 (Antonov et al., 2005; Garcia, 2005a,b; Locarnini et al., 2005), spaced 10° of latitude apart and approximately coinciding with the cruise track on which the samples for this study were collected (color coding in panel **d**). Additionally overlaid as coloured X's are the point definitions of the 11 water types discerned in this study. Where two water types constitute a water mass, the water types are connected with a thick coloured line for clarity. For abbreviations please refer to tables S2 and S3.

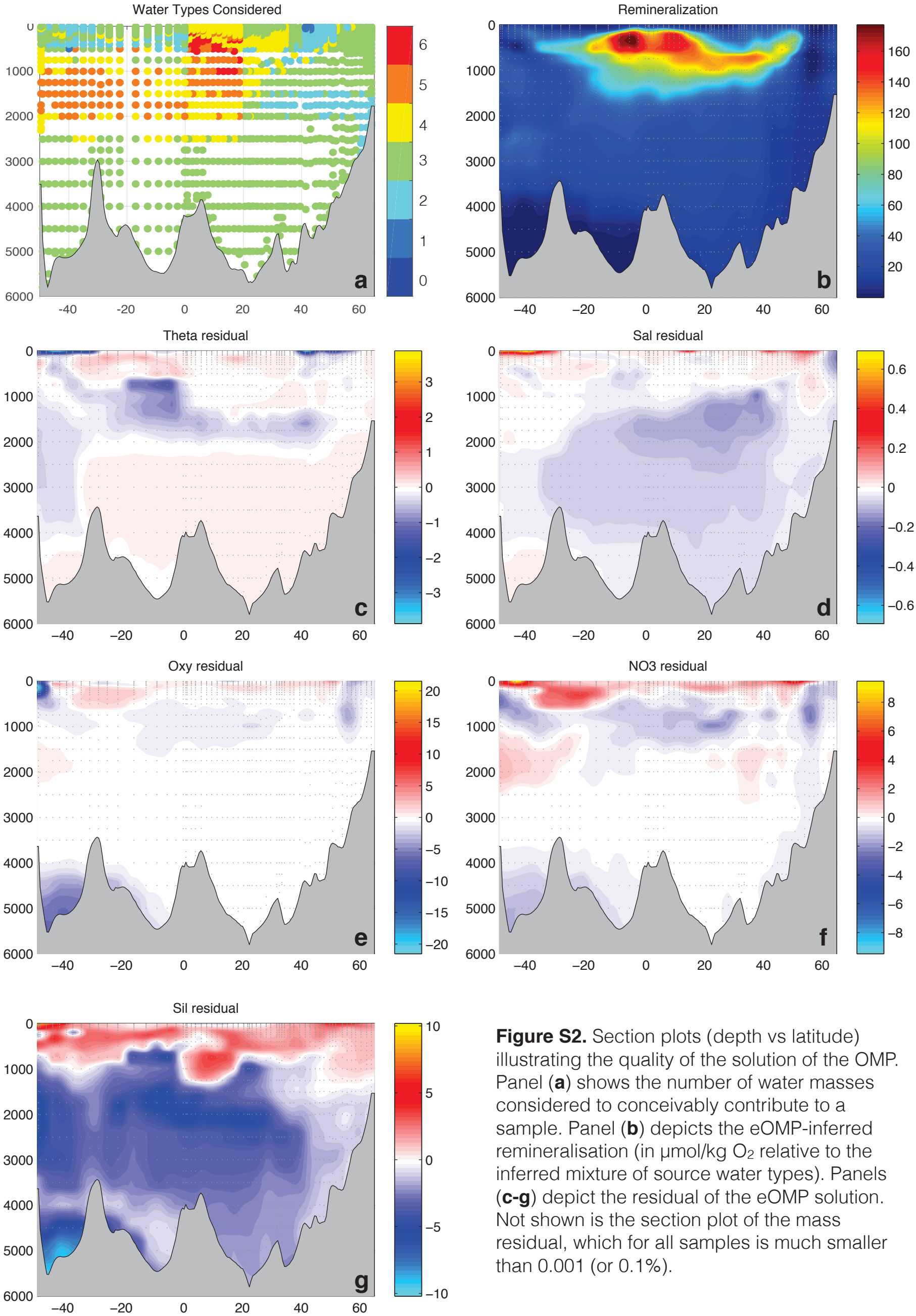

Figure S2. Section plots (depth vs latitude) illustrating the quality of the solution of the OMP. Panel (**a**) shows the number of water masses considered to conceivably contribute to a sample. Panel (**b**) depicts the eOMP-inferred remineralisation (in µmol/kg O_2 relative to the inferred mixture of source water types). Panels (**c-g**) depict the residual of the eOMP solution. Not shown is the section plot of the mass residual, which for all samples is much smaller than 0.001 (or 0.1%).

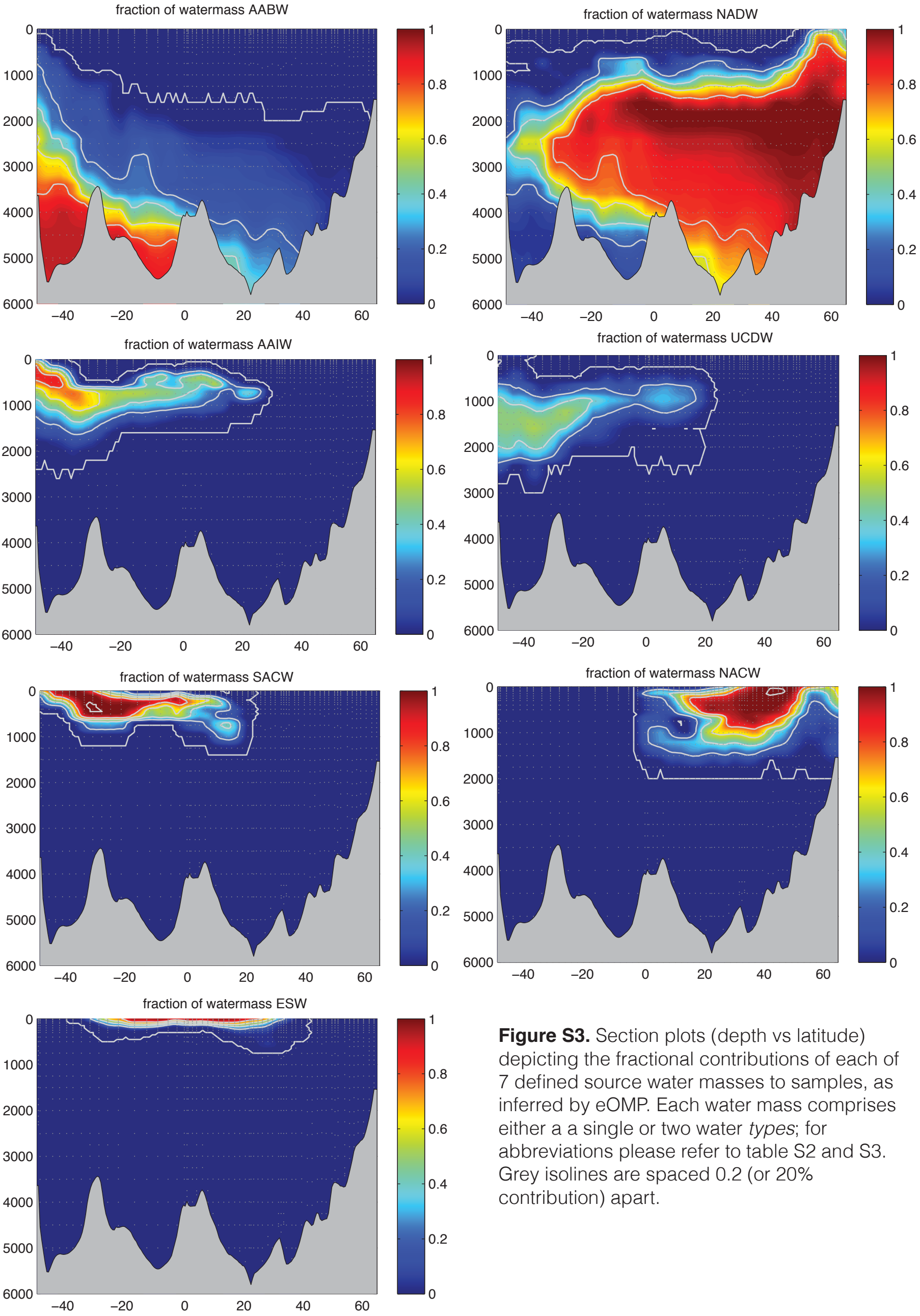

Figure S3. Section plots (depth vs latitude) depicting the fractional contributions of each of 7 defined source water masses to samples, as inferred by eOMP. Each water mass comprises either a a single or two water *types*; for abbreviations please refer to table S2 and S3. Grey isolines are spaced 0.2 (or 20% contribution) apart.

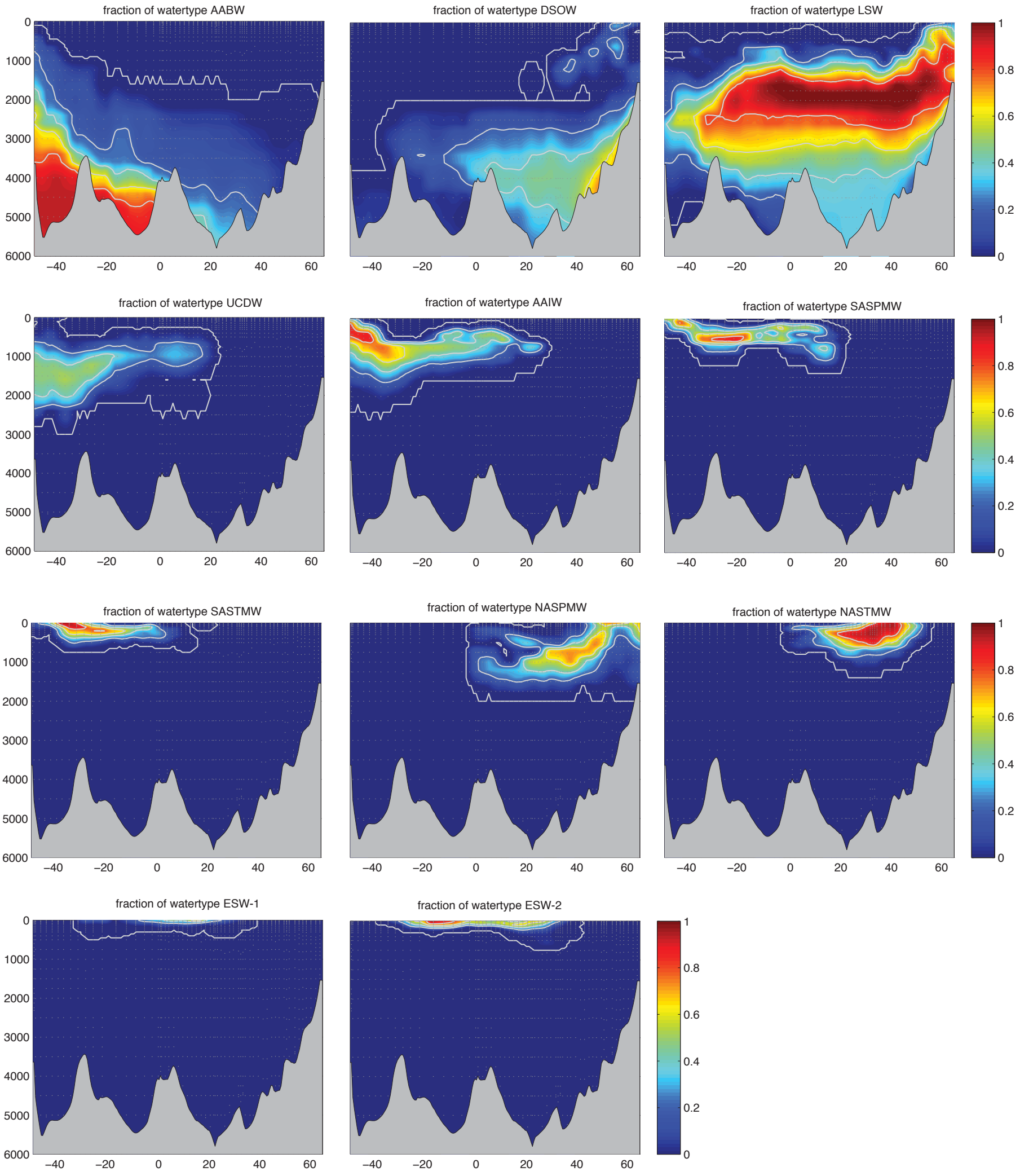

Figure S4. Section plots (depth vs latitude) depicting the fractional contributions of each of 11 defined source water types to samples, as inferred by eOMP. Grey isolines at spaced 0.2 (or 20% contribution) apart. For abbreviations please refer to tables S2 and S3.

References

Antonov, J.I., Locarnini, R.A., Boyer, T.P., Mishonov, A.V., Garcia, H.E., 2006. World Ocean Atlas 2005, Volume 2: Salinity. In: S. Levitus (Ed.), NOAA Atlas NESDIS 62. U.S. Government Printing Office, Washington, D.C. 182 pp.

Garcia, H.E., Locarnini, R.A., Boyer, T.P., Antonov, J.I., 2006a. World Ocean Atlas 2005, Volume 3: Dissolved Oxygen, Apparent Oxygen Utilization, and Oxygen Saturation. In: S. Levitus (Ed.), NOAA Atlas NESDIS 63. U.S. Government Printing Office, Washington, D.C. 342 pp.

Garcia, H.E., Locarnini, R.A., Boyer, T.P., Antonov, J.I., 2006b. World Ocean Atlas 2005, Volume 4: Nutrients (phosphate, nitrate, silicate). In: S. Levitus (Ed.), NOAA Atlas NESDIS 64. U.S. Government Printing Office, Washington, D.C. 396 pp.

Hood, E.M., Sabine, C.L., Sloyan, B.M., 2010. The GO-SHIP Repeat Hydrography Manual: A Collection of Expert Reports and Guidelines. IOCCP Report Number 14. ICPO Publication Series 134, Available online at http://www.go-ship.org/HydroMan.html.

Locarnini, R.A., Mishonov, A.V., Antonov, J.I., Boyer, T.P., Garcia, H.E., 2006. World Ocean Atlas 2005, Volume 1: Temperature. In: S. Levitus (Ed.), NOAA Atlas NESDIS 61. U.S. Government Printing Office, Washington, D.C. 182 pp.

Middag, R., de Baar, H.J.W., Laan, P., Cai, P.H., van Ooijen, J.C., 2011. Dissolved manganese in the Atlantic sector of the Southern Ocean. Deep-Sea Research Part Ii-Topical Studies in Oceanography 58, 2661-2677.

Middag, R., Séférian, R., Conway, T.M., John, S.G., Bruland, K.W., de Baar, H.J.W., 2015. Intercomparison of dissolved trace elements at the Bermuda Atlantic Time Series station. Mar. Chem. 177, Part 3, 476-489.

Rijkenberg, M.J.A., de Baar, H.J.W., Bakker, K., Gerringa, L.J.A., Keijzer, E., Laan, M., Laan, P., Middag, R., Ober, S., van Ooijen, J., Ossebaar, S., van Weerlee, E.M., Smit, M.G., 2015. “PRISTINE”, a new high volume sampler for ultraclean sampling of trace metals and isotopes. Mar. Chem. 177, Part 3, 501-509.

Tomczak, M., 1999. Some historical, theoretical and applied aspects of quantitative water mass analysis. J. Mar. Res. 57, 275-303.